



INTELLECTUAL PROPERTY  
402-391-4448

10-04-04

IFW

JAMES D. WELCH  
ATTORNEY AT LAW  
PROFESSIONAL ENGINEER

BEST AVAILABLE COPY

10328 PINEHURST AVE.  
OMAHA, NEBRASKA 68124

October 1, 2004

Commissioner for Patents  
Box: 1450  
Alexandria, AV 22313-1450

RE: OPPOSITION TO PUBLISHED APPLICATION OF NIKOONAHAD ET AL.  
TITLED "OPTICAL SYSTEM FOR MEASURING SAMPLES USING SHORT  
WAVELENGTH RADIATION";  
SERIAL NO.: 10/718,126;  
FILE DATE: NOV. 19, 2003;  
PUB. NO.: US2004/0150820.

Dear Sir;

Please find enclosed a Check for \$180.00 and Ten (10)  
Publications which we feel the Examiner should consider in the  
Examination.

PATENTS:

PATENT NO. 6,222,199, ISSUED APR. 24, 2001; SERIAL NO.  
09/318,035, FILED MAY 25, 1999; INVENTOR FREEOUF.  
PATENT NO. 5,818,596, ISSUED OCT 6, 1998; SERIAL NO. 922,756,  
FILED SEP. 3, 1997; INVENTOR IMAI ET AL.  
PATENT NO. 6,323,947, ISSUED NOV. 27, 2001; SERIAL NO.  
09/461,658, FILED DEC. 14, 1999; INVENTOR FREEOUF.  
PATENT NO. 4,322,165, ISSUED MAR. 30, 1982; SERIAL NO. 14,408,  
FILED FEB. 23, 1979; INVENTOR ELLEBRACHT ET AL.  
PUBLISHED APPLICATION NO. US2002/0149774, PUB. DATE OCT. 17,  
2002; SERIAL NO. 10/027,385, FILED DEC. 21, 2001,  
INVENTOR McANINCH.  
PUBLISHED APPLICATION NO. US2003/0071996, PUB. DATA APR. 17,  
2003; SERIAL NO. 10/141,267 FILED MAY 8, 2002, INVENTOR  
WANG ET AL.  
PUBLISHED APPLICATION NO. US2003/0150997, PUB. DATE AUG. 14,  
2003; SERIAL NO. 09/780,124 FILED FEB. 9, 2001;  
INVENTOR ECKERT ETAL.

ARTICLES:

"OVERVIEW OF VARIABLE ANGLE SPECTROSCOPIC ELLIPSOMETRY (VASE),  
PART II: ADVANCED APPLICATIONS", JOHS ET AL., SOC. PHOTO-OPTICAL  
INSTRU. ENG., 1999.

"OPTICAL CHARACTERIZATION IN VACUUM ULTRAVIOLET WITH VARIABLE

10/06/2004 SSITHIB1 00000089 10718126


180.00 OP

01 FC:1806

ANGEL SPECTROSCOPIC ELLIPSOMETRY: 157 NM AND BELOW", HILFIKER ET AL., METROLOGY, INSPECTION AND PROCESS CONTROL FOR MICROLITHOGRAPHY, 2000.

I attest that a copy of the accompanying materials was sent to Applicant's Attorney: Parsons Hsue and De LLP, at 655 Montgomery St., San Francisco, CA 94111 with First Class Postage affixed on October 1, 2004.

Sincerely,

  
JAMES D. WELCH

JW/hs

enc.



JAMES D. WELCH  
ATTORNEY AT LAW  
PROFESSIONAL ENGINEER

INTELLECTUAL PROPERTY  
402-391-4448

10328 PINEHURST AVE.  
OMAHA, NEBRASKA 68124

October 1, 2004

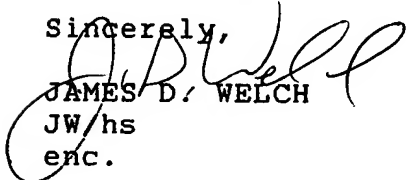
Parsons Hsue and De LLP  
655 Montgomery St.  
San Francisco, CA 94111

RE: OPPOSITION TO PUBLISHED APPLICATION OF NIKOONAHAD ET AL.  
TITLED "OPTICAL SYSTEM FOR MEASURING SAMPLES USING SHORT  
WAVELENGTH RADIATION";  
SERIAL NO.: 10/718,126;  
FILE DATE: NOV. 19, 2003;  
PUB. NO.: US2004/0150820.

Dear Sirs;

Enclosed please find copies of materials we feel should be  
considered by the Examiner during Prosecution of the identified  
case, and which have been provided to the Patent Office.

Sincerely,

  
JAMES D. WELCH

JW/hs

enc.

**REPRINT**

Critical Reviews of  
Optical Science  
and Technology



**Volume CR72**

**Overview of Variable Angle Spectroscopic  
Ellipsometry (VASE), Part II:  
Advanced Applications**

from

**Optical Metrology**

Copyright 2000 Society of Photo-Optical Instrumentation Engineers.

This paper was published in *Critical Reviews of Optical Science and Technology Volume CR72* (proceedings of a conference held 1 March 2000 in Denver, Colorado, ©1999 by SPIE, Bellingham, WA) and is made available as an electronic reprint with permission of SPIE. Single print or electronic copies for personal use only are allowed. Systematic or multiple reproduction, or distribution to multiple locations through an electronic listserver or other electronic means, or duplication of any material in this paper for a fee or for commercial purposes is prohibited. By choosing to view or print this document, you agree to all the provisions of the copyright law protecting it.

**Proceedings of a conference held**

18-19 July 1999

Denver, Colorado

©1999 by the Society of Photo-Optical Instrumentation Engineers  
Box 10, Bellingham, WA 98227 USA. Telephone 360/676-3290.

# Overview of Variable Angle Spectroscopic Ellipsometry (VASE), Part II: Advanced Applications

Blaine Johs\*, John A. Woollam, Craig M. Herzinger, James Hilfiker,  
Ron Synowicki, and Corey L. Bungay

J.A. Woollam Co., Inc., 645 'M' St. #102, Lincoln, NE 68508

## ABSTRACT

A preceding companion paper provides a general introduction to Variable Angle Spectroscopic Ellipsometry (VASE), and also describes many typical applications of the technique. In this paper, more advanced VASE applications are discussed. These applications rely on recent advances in ellipsometric hardware, which allow extremely accurate ellipsometric data to be acquired over a broad spectral range, from the IR to VUV. This instrumentation can also quantitatively measure the optical response of non-isotropic samples. Advanced data analysis techniques are also presented.

**Keywords:** ellipsometry, advanced instrumentation, parametric models, multi-sample analysis, depolarization, anisotropy, Mueller matrix.

## 1. ADVANCED INSTRUMENTATION

One of the principal advantages of the ellipsometric technique is its potential for highly *precise* and *accurate* measurements. As ellipsometry measures a ratio quantity (Equation 1), the measurement is potentially more precise and accurate than a traditional intensity reflectance or transmission measurement (the precision and accuracy of intensity-based optical measurements can be hindered by baseline intensity drifts, difficulties in reproducibly collecting all of the measurement beam, and imperfect reference samples). On the other hand, since ellipsometry is a polarization-based measurement, relatively complex optical instrumentation is required (as compared to a simple intensity measurement; see Figure 1), and acquiring highly *accurate* ellipsometric data over wide spectral and angle ranges is not trivial.

### Definition of ellipsometric parameters $\Psi$ and $\Delta$ :

( $r_p$  and  $r_s$  are the complex Fresnel reflectivities  
for p- and s- polarized light)

$$\tan(\Psi) \cdot e^{i\Delta} = \frac{r_p}{r_s} \quad (1)$$

When constructing a Variable Angle Spectroscopic Ellipsometer (VASE) system, ideal optical elements, namely polarizers and compensators, are desirable. An ideal optical

---

\* Correspondence: Email: [bjohs@jwoollam.com](mailto:bjohs@jwoollam.com); [www.jwoollam.com](http://www.jwoollam.com);  
Telephone: 402-477-7501; FAX: 402-477-8214

element should impart a well defined polarization state to the probe beam over the spectral range of the instrument, and have minimal angular alignment sensitivity. Imperfect optical elements can also be utilized in ellipsometric instrumentation (and in fact they are an unfortunate necessity in some spectral ranges and instrument designs), but the non-idealities must be accurately characterized and accounted for in the data acquisition scheme to ensure accurate ellipsometric data. Furthermore, it is also necessary to accurately calibrate the ellipsometer system to determine the azimuthal orientation of the optical elements with respect to the sample plane of incidence. While a comprehensive discussion is beyond the scope of this article, numerous references<sup>1,2,46</sup> provide excellent overviews of traditional ellipsometric instrumentation and calibration procedures. In this section, recent state-of-the-art ellipsometric instrumentation which provides extremely accurate spectroscopic data is described, along with applications which exploit this advanced capability.

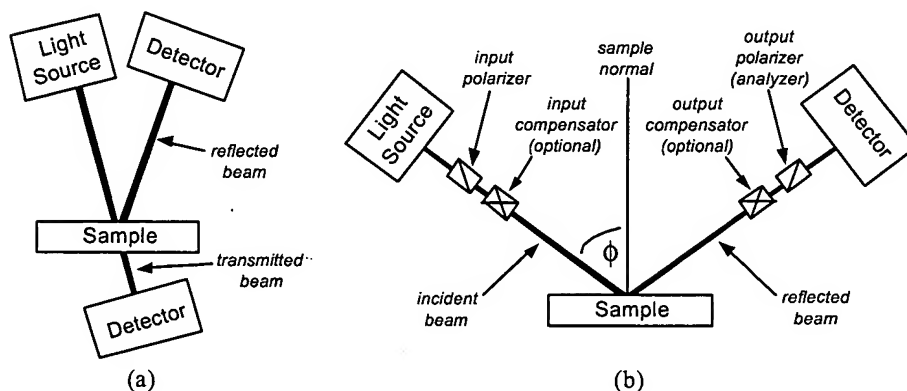


Figure 1. Basic components required for typical optical measurements: (a) near normal incidence intensity reflection and transmission instrumentation, (b) ellipsometric instrumentation for measurement at oblique angle of incidence ' $\phi$ '; the optical elements (polarizers and optional compensators) can be fixed, adjustable, continuously rotating, or electrically modulated depending on the particular ellipsometer configuration.

### 1.1. Compensator-based ellipsometer designs

The Rotating Analyzer Ellipsometer (RAE) configuration (and its counterpart, the Rotating Polarizer Ellipsometer (RPE) configuration) is commonly employed in spectroscopic ellipsometry systems. This relatively simple ellipsometer configuration requires only two polarizers, and since essentially ideal crystal polarizers are readily available, it is reasonably straight forward to build a high accuracy spectroscopic RAE or RPE system<sup>2</sup> which operates in the UV-VIS-NIR spectral range (190 – 1700 nm). However, there are well know limitations to this simple spectroscopic ellipsometer configuration<sup>3</sup>: 1) the 'handedness' of the ellipsometric  $\Delta$  parameter can not be uniquely determined ( $\Delta$  can range from 0 – 360°, but for  $\Delta > 180^\circ$ , an RAE or RPE system will report  $\Delta_{\text{RAE}} = 360^\circ - \Delta_{\text{actual}}$ ), and 2) the precision and accuracy of the RAE or RPE measured  $\Delta$  value is poor when  $\Delta$  is near 0° or 180°. These limitations may be inconsequential for many applications, but for some samples (very thin dielectric films on glass, for example), very accurate measurements of  $\Delta$  are required for adequate characterization of the sample.

Other ellipsometer configurations may not suffer from the aforementioned ‘ $\Delta$ ’ limitations, but they incur other tradeoffs. Null ellipsometer systems, for example, measure  $\Psi$  and  $\Delta$  with high precision and accuracy over the entire measurement range; however, for various reasons, the null configuration is not generally employed in spectroscopic systems. Phase modulation ellipsometer (PME) systems measure  $\Delta$  accurately over the full  $0 - 360^\circ$  range, but suffer from  $\Psi$  accuracy problems when  $\Psi$  is near  $0^\circ$  or  $45^\circ$ , depending on the particular instrument configuration<sup>4</sup> (this limitation can be overcome by the additional complexity of a dual channel detection system<sup>5</sup>). The photoelastic modulator used in PME ellipsometer systems are inherently chromatic optical elements, and the drive voltage must be accurately adjusted at each wavelength during a spectroscopic scan. Furthermore, due to the high modulation frequency, it is not possible to construct a PME system which simultaneously acquires spectroscopic ellipsometric data (implementing true parallel signal acquisition and readout) with existing diode array spectrometer technology.

#### 1.1.1. Rotating Analyzer Ellipsometer (RAE) with Adjustable Retarder

In theory, the RAE and RPE ‘ $\Delta$ ’ measurement limitations can be eliminated by simply adding a compensator to the beam path (either before or after the sample). However, this is more challenging than it sounds, for several reasons: 1) a perfectly ideal spectroscopic compensator element does not exist, 2) compensator elements which can be used spectroscopically (such as Fresnel Rhombs) are only pseudo-achromatic, bulky, and difficult to align, and 3) if the retardance of the compensator is not meticulously calibrated (throughout the entire spectral range), or if the compensator is not properly aligned, the accuracy of the ellipsometric data will be degraded (instead of enhanced) by the introduction of the compensator element.

In spite of these challenges, one commercially available ellipsometer system does successfully integrate a compensating element with a high accuracy RAE<sup>7</sup>. In this system, a computer controlled  $\text{MgF}_2$  Berek waveplate is used to accurately introduce retardance into the beam path<sup>8</sup>. Since the retarder is under computer control, it is possible to generate appropriate retardance values ( $0 - 90^\circ$ ) over a broad ( $150 - 1700 \text{ nm}$ ) spectral range. Figures 2 - 4 show examples of variable angle and spectroscopic ellipsometric data which were acquired with such a system. In these examples, it is the accurate measurement of the ellipsometric  $\Delta$  parameter near  $0^\circ$  and  $180^\circ$  which enables a determination of the thickness and index of a dielectric film deposited on a polycarbonate substrate, and the optical constants and surface roughness layer on a glass microscope slide. A depolarization measurement of the glass microscope slide is also shown in Figure 4. This is another capability provided by the addition of the adjustable retarder, and is discussed in more detail in section 3.2.

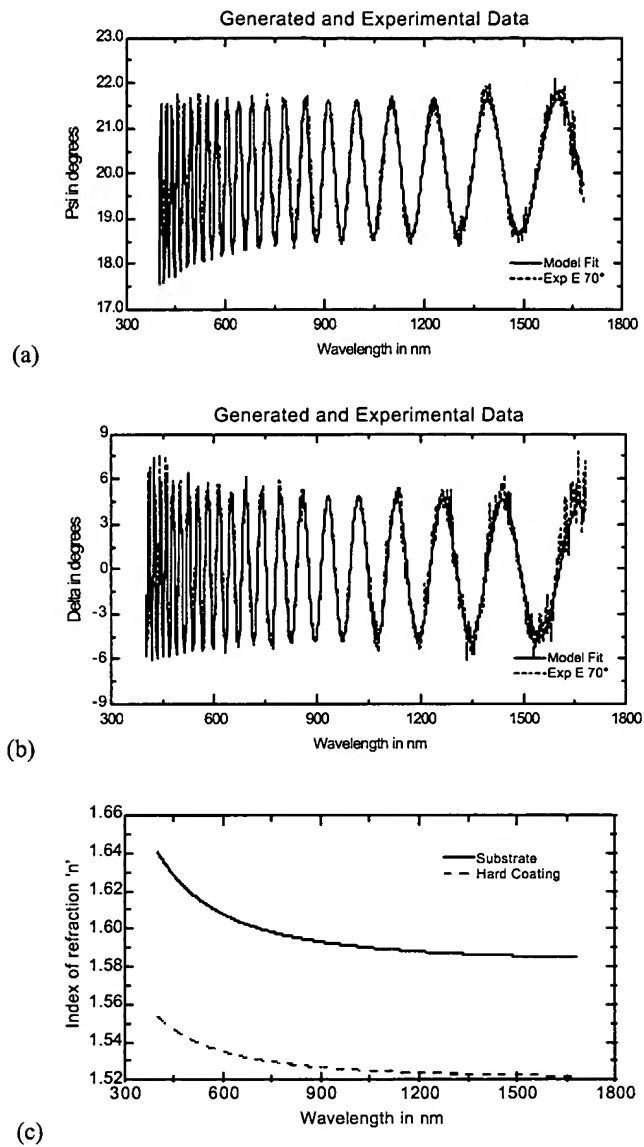


Figure 2. Ellipsometric  $\Psi$  (a) and  $\Delta$  (b) data acquired with a retarder-equipped RAE system<sup>7</sup> on a polycarbonate lens with a thick ( $4.35\mu\text{m}$ ) hard coating. Accurate measurement of the period and amplitude of oscillations in both  $\Psi$  and  $\Delta$  enabled accurate determination of the film thickness and optical constants (c).



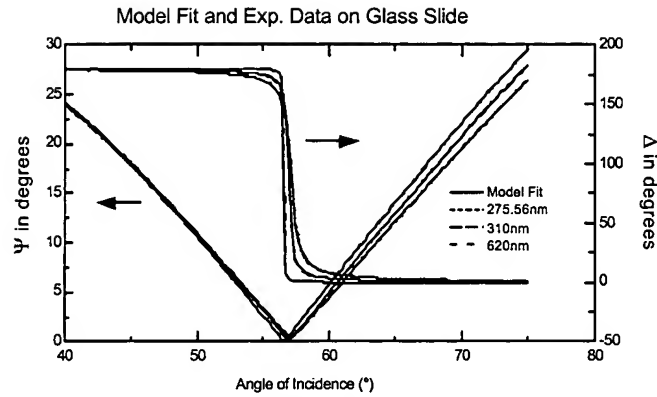


Figure 3. Accurate measurement of variable angle ellipsometric data near the Brewster angle on a glass microscope slide, using an RAE system with an adjustable retarder<sup>7</sup>. To achieve the near perfect data fits shown in the graph, it was necessary to add 23Å of surface roughness to the front and back surfaces of the glass in the optical model. The more rounded  $\Delta$  curves correspond to the shorter wavelength data, where the glass is more absorbing.

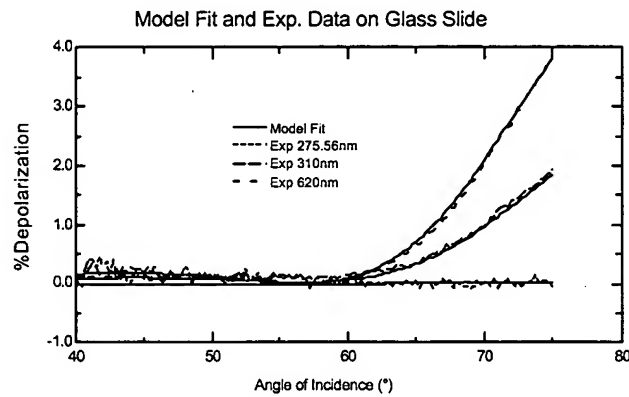


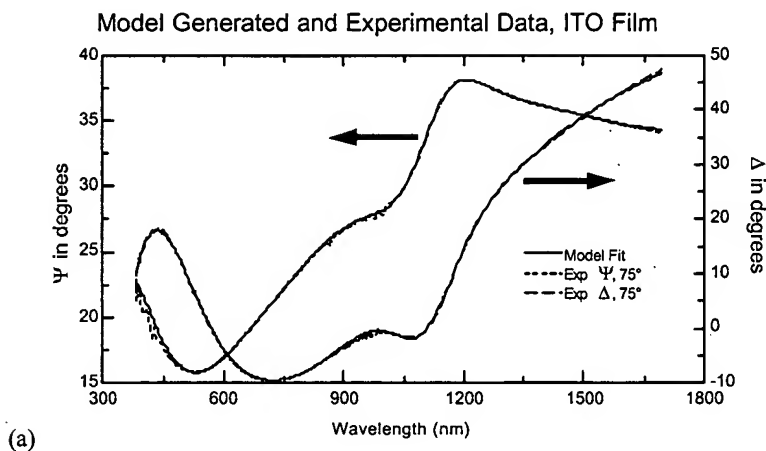
Figure 4. Depolarization measurement of a glass microscope slide with a retarder-equipped RAE system<sup>7</sup>. The depolarization is caused by the backside reflection of the slide; as the glass becomes opaque at shorter wavelengths, the depolarization goes to zero.

### 1.1.2. Rotating Compensator Ellipsometer (RCE) Configuration

Another approach to introducing a compensator into the ellipsometer beam path is to implement the Rotating Compensator Ellipsometer (RCE) configuration. There are many advantages to the RCE configuration, including<sup>9</sup>: accurate measurement of the ellipsometric  $\Psi$  and  $\Delta$  parameters over the complete measurement range ( $\Psi=0-90^\circ$ ,  $\Delta=0-360^\circ$ ), no residual input or output polarization sensitivity (due to a fixed polarizer on input, and a fixed analyzer on the output), and the capability to directly measure depolarization effects. However, only recently have Spectroscopic RCE systems been constructed<sup>10-14</sup>. The prior lack of spectroscopic RCE systems, in spite of the well known advantages to this configuration, was mainly due to the perceived difficulty of constructing a mechanically rotatable compensator element which behaves ideally (retardance  $\approx 90^\circ$ ) over a wide spectral range. Recently, this challenge has been

successfully addressed in a number of ways: 1) a special rhomb-like prism retarder has been used to implement a Fourier Transform Infra Red (FTIR) RCE system<sup>15</sup> (data from which will be shown in the IR-VASE section of this paper), 2) a realization that ellipsometric data can still be acquired (albeit with reduced  $\Delta$  measurement capability) even as the retardance of the compensator passes through  $180^\circ$  in part of the spectrum<sup>11</sup> (which is inevitable when using standard waveplates for compensator elements, as their retardance exhibits a  $1/\lambda$  dependence), and 3) development of multi-element, pseudo-achromatic compensators coupled with a rigorous calibration methodology<sup>16</sup>. A commercially available spectroscopic RCE instrument is based on approach #3<sup>14</sup>. This instrument also employs a diode array spectrometer (Diode Array Rotating Compensator Ellipsometer, or DARCE), such that simultaneous acquisition of spectroscopic ellipsometric data is possible<sup>17</sup>. In addition, by switching the light source and/or diode array detector, it is possible to cover a variety of spectral ranges, from the DUV (190 nm) to the NIR (1700 nm).

Figure 5 shows ellipsometric data which was acquired on an ITO film with a VIS-NIR DARCE system<sup>14</sup>. In this system, a quartz tungsten halogen (QTH) light source was directly coupled into the DARCE input optics, and a bifurcated collection fiber split the output beam into two diode array spectrometers: a Si-based array covering the 400-1000nm spectral range, and an InGaAs-based array covering the 1000-1700nm spectral range. Data is simultaneously acquired on both diode arrays, such that a 1-2 second acquisition time results in ellipsometric data covering the 400-1700nm spectral range with excellent precision and accuracy. Characterization of flat panel display materials, such as Indium Tin Oxide (ITO) and thick amorphous Si films, is greatly enhanced by ellipsometric measurements in this NIR spectral range<sup>18</sup>. Likewise, the communications industry which utilizes optics and coatings that operate near 1.3 and 1.5  $\mu\text{m}$  would greatly benefit from fast spectroscopic ellipsometric material characterization in this VIS-NIR spectral range.



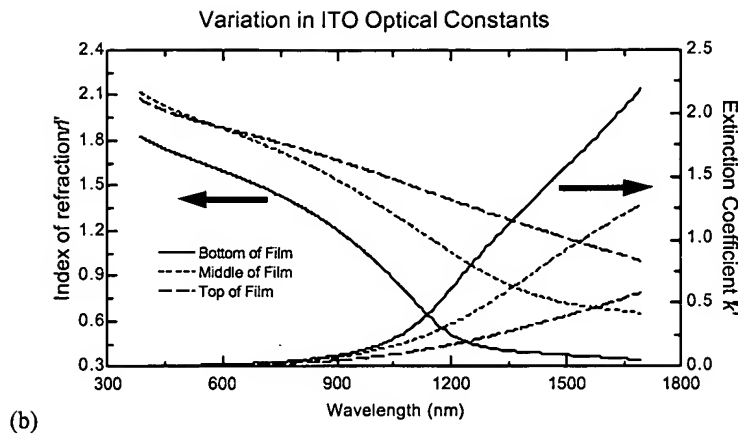


Figure 5. (a) DARCE data acquired on an Indium Tin Oxide (ITO) coating on glass sample; note the accurate ' $\Delta$ ' measurements near  $0^\circ$ . (b) ITO optical constants resulting from analysis of the data shown in (a), using a graded optical model; note the variation in free-carrier optical absorption in the NIR spectral range (1000-1700 nm). The optical absorption is directly related to the electrical conductivity of the film, which is critical for flat panel display applications and highly dependent on the annealing process.

### 1.2. Verification of Ellipsometric Accuracy: Straight-Through (Air) Measurements

Verifying the accuracy of an ellipsometric system is not a simple matter. Reference standards have been proposed<sup>19</sup>, however, preparing a sample which exhibits reproducible optical properties to the level of precision offered by a typical Spectroscopic Ellipsometer system is not feasible in most laboratories, let alone a manufacturing environment. Reference  $\text{SiO}_2$  on Si wafers are available from NIST and other companies; however, the precision of most ellipsometer systems is still much better than the tolerance of the reference standards (and the reference standards may also change over time). Even the optical constants and model for  $\text{SiO}_2$  on Si structures, which is arguably the most well studied material system by ellipsometry, are still a subject of discussion in the literature<sup>20,21</sup>.

The only material for which the ellipsometric parameters are absolutely known is 'Air': an ellipsometric measurement in the straight-through configuration should by definition return  $\Psi=45^\circ$  and  $\Delta=0^\circ$ . A straight-through measurement is a 'necessary but not sufficient' accuracy criteria for an ellipsometer system: accurately measuring  $\Psi=45^\circ$  and  $\Delta=0^\circ$  in the straight-through configuration does not guarantee that the ellipsometer will also measure accurate ellipsometric data on general samples, but any deviations from ideal behavior observed in straight-through measurements certainly imply that measurement errors will be present in ellipsometric data acquired on real samples as well.

Figure 6 shows straight-through measurement data which was acquired using commercially available Spectroscopic Ellipsometer systems utilizing compensators<sup>7,13,14</sup> over a broad spectral range (190nm - 40 $\mu\text{m}$ ). Note that the deviations in the measured data from the ideal values is much less than  $0.1^\circ$  over most of the entire range. As some papers<sup>22</sup> report straight-through  $\tan(\Psi)$  and  $\cos(\Delta)$  measurements (which should both be

exactly 1.0), Figure 7 plots the data from Figure 6 transformed into  $\tan(\Psi)$  and  $\cos(\Delta)$ . Note that for a compensator-based ellipsometer system which can accurately measure  $\Delta$  near  $0^\circ$ , the  $\cos(\Delta)$  parameter becomes ridiculously close to 1.0.

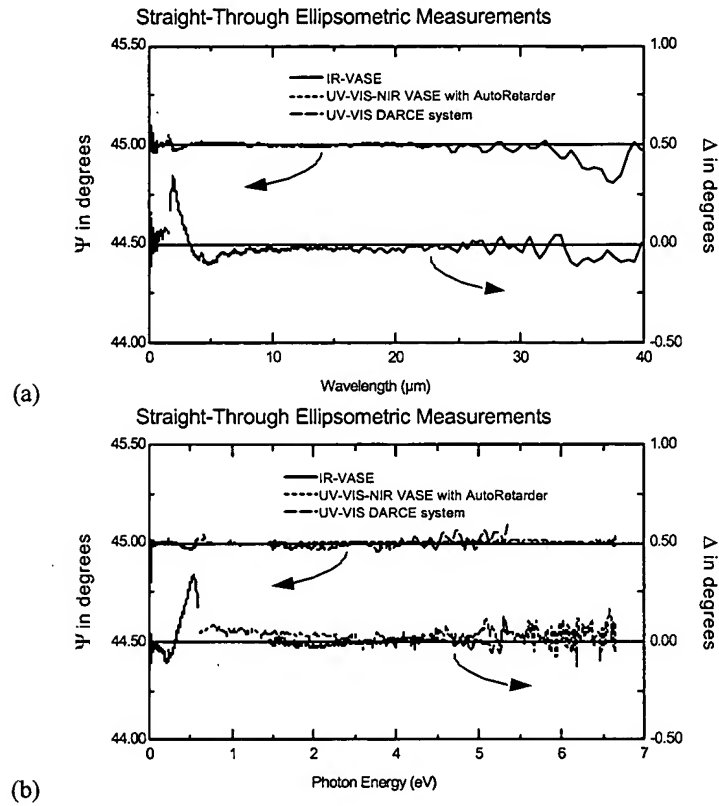
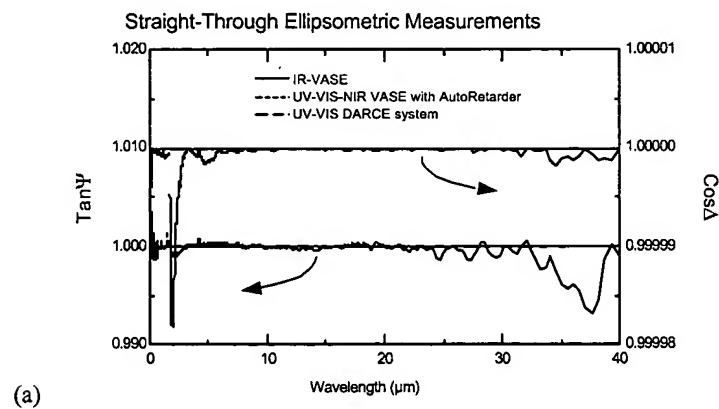


Figure 6. Straight-through ellipsometric measurements of 'air' performed on commercially available Spectroscopic Ellipsometer systems <sup>7,13,14</sup>, plotted in wavelength (a), and photon energy (b). For an ideal system,  $\Psi=45^\circ$  and  $\Delta=0^\circ$  for this measurement.



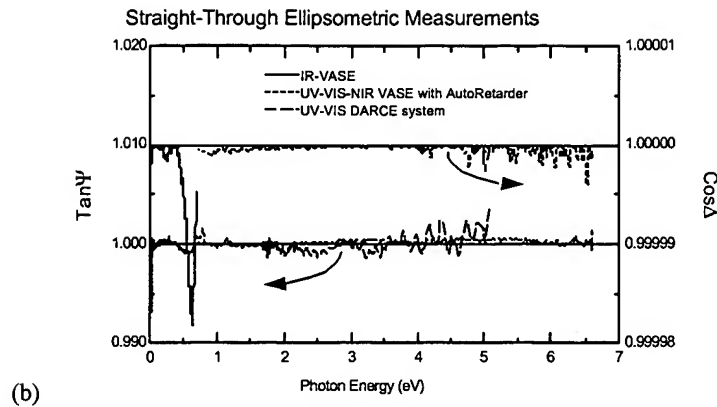


Figure 7. Straight-through ellipsometric measurements of 'air' performed on commercially available Spectroscopic Ellipsometer systems<sup>7,13,14</sup>, transformed into  $\tan(\Psi)/\cos(\Delta)$  notation and plotted in wavelength (a), and photon energy (b). For an ideal system,  $\tan(\Psi)=\cos(\Delta)=1.0$  for this measurement.

## 2. ADVANCED DATA ANALYSIS TECHNIQUES

When analyzing ellipsometric data from a sample which consists of materials with well known optical constants, it is very straight forward to build an optical model for the sample, and perform regression analysis of the data to extract layer thicknesses and surface/interfacial roughness<sup>23</sup>. However, for many (if not most) materials, optical constants are not well known or may vary, depending on the material preparation method (the term 'optical constant' is somewhat of a misnomer). Therefore, extracting accurate material optical constants is an important component of ellipsometric data analysis. For ideal bulk or single layer structures, it is possible to directly invert optical constants 'n' and 'k' from the ellipsometric parameters  $\Psi$  and  $\Delta$ . For more complicated structures which include multiple layers, non-ideal interfaces, or gradients in the film optical properties, advanced data analysis techniques are required to simultaneously and uniquely extract optical constants (sometimes of multiple materials) and structural information (film thicknesses, surface/interfacial roughness, grading profile) from the VASE data.

### 2.1. Optical Constant Parameterization by GBPS

VASE measurements are typically performed over a wide spectral range, and for quantitative analysis of the data, it is necessary to specify material optical constants over the complete spectral range of the data. Of course, it is always possible to describe the dispersion in optical constants by a tabulated list of 'n' and 'k' values (or equivalently, the real and imaginary parts of the dielectric function,  $\epsilon_1$  and  $\epsilon_2$ ) at discrete wavelengths (and interpolating within the table as necessary). However, such a tabulated list requires large number of parameters (2X the number of wavelengths in the data set), and does not enforce any Kramers-Kronig (K-K) consistency between the real and imaginary parts of the dielectric function<sup>24</sup>. A parametric dispersion model enables the calculation of

material optical constants as a function of wavelength, using a much smaller set of free parameters. The literature contains many parametric dispersion models which are useful in the analysis of ellipsometric data, including Cauchy, Sellmeier, Harmonic Oscillators<sup>25</sup>, Tauc-Lorentz<sup>26</sup>, and others<sup>27-29</sup>. For example, the Cauchy dispersion parameterization is shown in Equation (2). Many of the dispersion models are appropriate for only specific types of materials, for example, the Cauchy model is valid only for transparent materials, and the Tauc-Lorentz<sup>26</sup> works best for amorphous materials. In this section, a general Gaussian-Broadened Polynomial Superposition (GBPS) parametric dispersion model is described, which can be broadly applied to most materials including crystalline and amorphous semiconductors, metals, and organics.

$$n(\lambda) = A + \frac{B}{\lambda^2} + \frac{C}{\lambda^4}, \quad k(\lambda) = 0 \quad (2)$$

The details of the GBPS parametric dispersion model can be found elsewhere<sup>30</sup>, however, the model is fundamentally constructed by a superposition of piece-wise continuous polynomials which are numerically convolved with Gaussian oscillator lineshapes (see Figure 8). While this model does not attempt to directly capture the underlying physics of the material dielectric function, it does have a number of advantages when compared to other dispersion models: 1) the resulting dielectric function is K-K consistent, 2) the use of 'true' Gaussian broadening allows for complete transparency below the fundamental band gap, 3) it is flexible enough to represent the subtle nuances in dielectric function spectra which are often not adequately described by first principles physics-based models, 4)  $\epsilon_2$  is strictly positive (absorbing) for all positive frequencies, and 5) the parameterization is stable and robust, such that direct regression analysis of ellipsometric data is possible, and parameterized composition and temperature dependent dielectric function spectra can be readily constructed<sup>31</sup>.

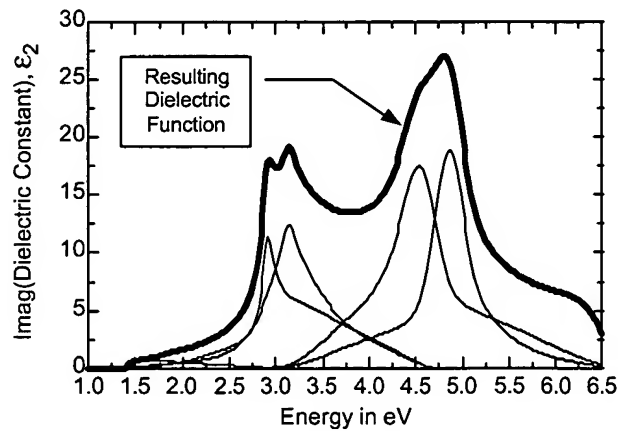
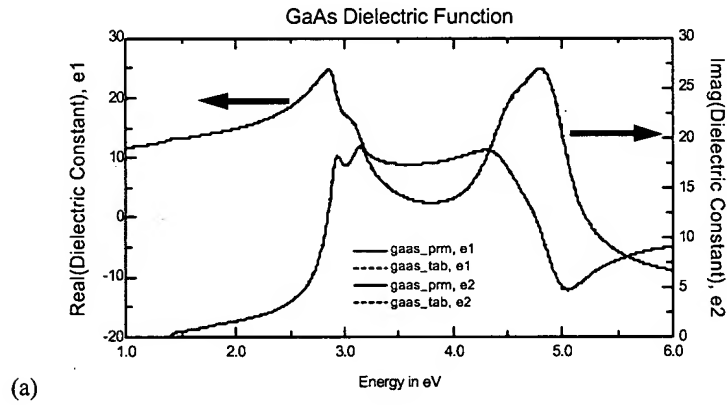
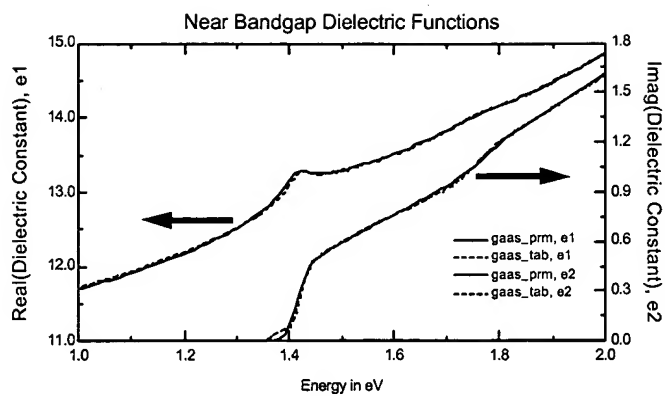


Figure 8. Construction of a GBPS parametric dielectric function representation by a summation of Gaussian-broadened polynomial segments (the resulting dielectric function in this figure is for GaAs, and is valid for  $E < 6\text{ eV}$ ).

To illustrate the ellipsometric data analysis capabilities provided by the GBPS parametric model, consider the following examples. Figure 9 shows the dielectric function of crystalline GaAs, which is accurately represented by the GBPS model with only 23 free parameters over the entire spectral range: below, at, and above the fundamental band gap. Figure 10 shows VASE data and extracted optical constants for a diamond-like carbon (DLC) film deposited on Si. To achieve this excellent level of agreement between the experimental and model fit data, only 5 fitting parameters were used: the DLC film thickness plus 4 parameters of the GBPS parameterized DLC optical constants. The ITO optical constants shown in Figure 5(b) were also parameterized by the GBPS model, enabling a simultaneous determination of the film optical constants, layer thickness, and grading profile.

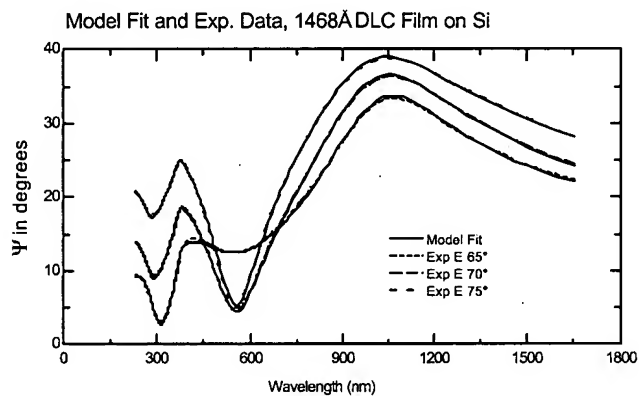
In summary, optical constant parameterization is a powerful technique for analyzing VASE data acquired on complex samples. By greatly reducing the number of parameters required to model the dispersion, material optical constants and structural information about the sample (such as layer thicknesses) can be simultaneously and uniquely determined. Utilizing optical constant parameterization in a multi-sample analysis (described in the next section) and over wide spectral ranges (also described in a subsequent section) further enhances the power of the technique. The GBPS model is a very general parametric dispersion model which can be applied to almost any material which exhibits optical absorption in the spectral range of the VASE measurement.



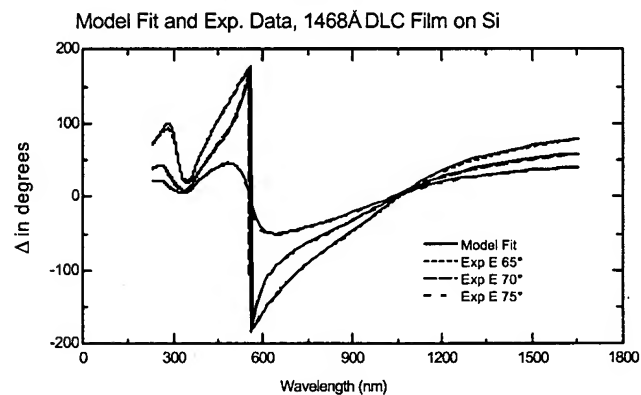


(b)

Figure 9. (a) Accurate parametric representation of the GaAs dielectric function over a wide spectral range; using the GBPS model with only 23 free parameters. (b) Blow-up of (a) comparing the tabulated values with the GBPS model near the GaAs fundamental band gap.



(a)



(b)



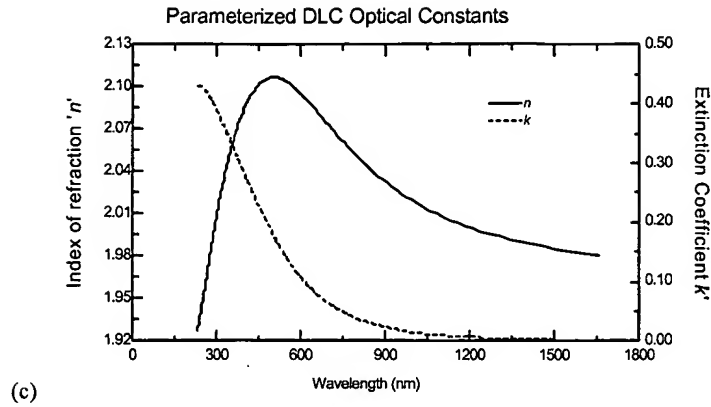


Figure 10. (a,b) Experimental VASE data and corresponding model fit data for a Diamond-like carbon (DLC) film deposited on Si; note the excellent model fits. (c) Optical constants extracted from the data in (a) and (b) using the GBPS parametric dielectric function model; only 4 adjustable parameters were required to describe the dispersion over the 230-1700nm spectral range.

## 2.2. Multi-Sample Analysis

If the optical constants for a given material are truly *constant*, then those same optical constants should accurately fit the VASE data acquired from any sample which includes the material. That is the premise behind the powerful multi-sample analysis technique. In this technique, VASE data from multiple samples are simultaneously included in the regression analysis, and a common set of optical constants is 'coupled' into the optical model used for each sample. By including samples with a range of layer thicknesses, the information content of the data set is greatly enhanced, enabling the simultaneous and accurate determination of all the layer thicknesses of the samples, and layer optical constants (sometimes for even more than one material). Each sample adds one additional thickness fit parameter to the analysis, but this is offset by the sample's VASE data, which may have been acquired over multiple angles and hundreds of wavelengths. The concept of simultaneously analyzing ellipsometric data from multiple samples has been routinely employed in the analysis of single wavelength ellipsometric data<sup>32</sup>. However, it seems to be under-utilized in VASE data analysis, possibly due to the added complication of handling multiple data sets in the optical modeling and regression software. The only fundamental requirement of the multi-sample technique is a systematic series of samples with material of uniform optical properties covering a range of layer thicknesses; this requirement can be readily achieved for many material systems.

The literature contains a number of good examples of multi-sample analysis of VASE data<sup>33,34</sup>. To illustrate this technique, we will present a multi-sample analysis consisting of SiO<sub>2</sub> on Si wafers, in which the Si and SiO<sub>2</sub> optical constants, along with SiO<sub>2</sub> and interfacial layer thicknesses, are simultaneously extracted. This analysis is based on the work of Herzinger<sup>21</sup>; in this example we have extended the spectral range of the ellipsometric measurements (and hence the optical constants) to 8.5 eV (see section 4.2 for a description of the VUV ellipsometer instrumentation). The four samples used for this example are described in Table I. Note that different angles, spectral ranges (covering NIR-VIS-UV-VUV), and resolutions were used for the ellipsometric data sets (higher resolution scans were used for the 1 μm thick film to better resolve the

interference fringes). Since a parametric representation was used for the optical constants (the Si optical constants used a GBPS parameterization, and a two term Sellmeier dispersion function was used for SiO<sub>2</sub>), it is not necessary that all data sets cover the same spectral range. To achieve the excellent model fits to the experimental data which are shown in Figures 11 – 14, an interfacial layer between the Si substrate and oxide film was required. The optical nature of this interface is thoroughly discussed elsewhere<sup>21,52</sup>, and in this work we treated the interfacial layer in the same manner: the interfacial layer optical constants were assumed to be transparent with a higher index than the oxide film (the index offset was taken from Ref. 21), and they were constrained to follow the same dispersion as the oxide film. The results of the multi-sample analysis are shown in Table I (layer thicknesses) and Figures 15 and 16 (optical constants). The Si and SiO<sub>2</sub> optical constants are self-consistent (by virtue of the multi-sample analysis), and they were determined without any special sample preparation (such as stripping the oxide, which can add uncertainties to the data analysis<sup>35,36</sup>).

Sample	Experimental Ellipsometric Data	Interface Thickness (Å)	SiO <sub>2</sub> Thickness (Å)
nominal 250Å thermal oxide on Si	0.75 - 6.0 by 0.01 eV, at 70°, 75°, 80°	8.9±1.5	253.1±1.2
native oxide on Si	4.2 - 8.5 by 0.05 eV, at 75.5°	10.6±2.5	10.9±3.1
nominal 280Å thermal oxide on Si	4.2 - 8.25 by 0.05 eV, at 75.5°	8.9±1.9	270.6±1.7
nominal 1µm thermal oxide on Si	4.7- 8.25 by 0.02 eV, at 75.5°	37.0±2.3	10474±10

Table I. Description of samples and resulting layer thicknesses from a multi-sample VASE analysis of SiO<sub>2</sub> on Si wafers. The '±' values on the thickness values are the 90% statistical confidence limits reported by the regression analysis of the data.

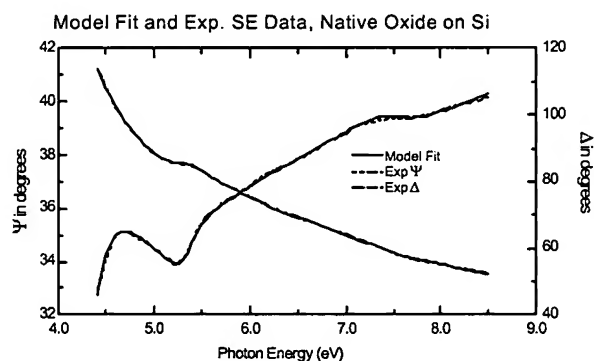


Figure 11. Model fit and experimental VUV spectroscopic ellipsometric data for the native oxide on Si sample which was part of a multi-sample analysis.

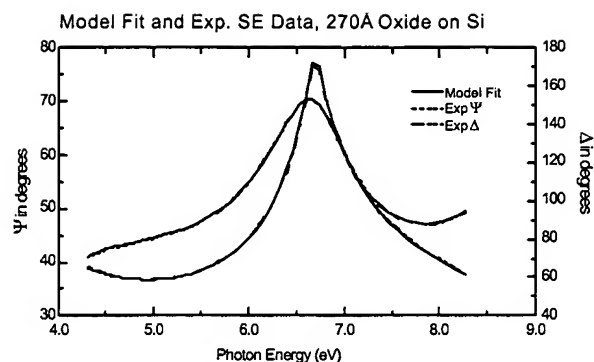


Figure 12. Model fit and experimental VUV spectroscopic ellipsometric data for the thermal oxide (nominally 270Å) on Si sample which was part of a multi-sample analysis.

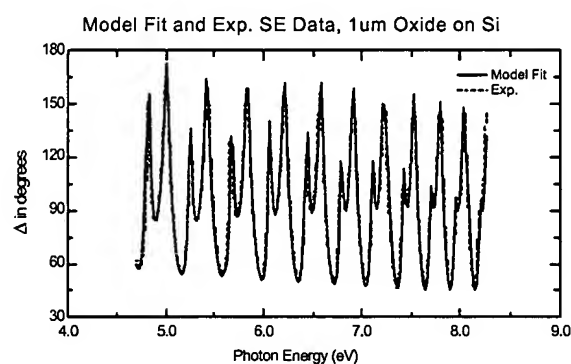


Figure 13. Model fit and experimental VUV spectroscopic ellipsometric data (only  $\Delta$  is shown for clarity) from the thick thermal (nominally 1µm) oxide on Si sample which was part of a multi-sample analysis.

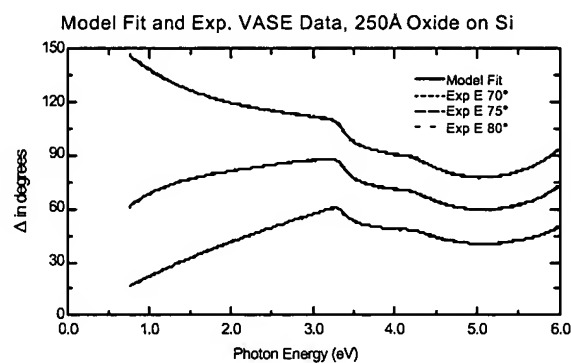


Figure 14. Model fit and experimental NIR-VIS-UV spectroscopic ellipsometric data (only  $\Delta$  is shown for clarity) from the thermal oxide on Si sample which was part of a multi-sample analysis.

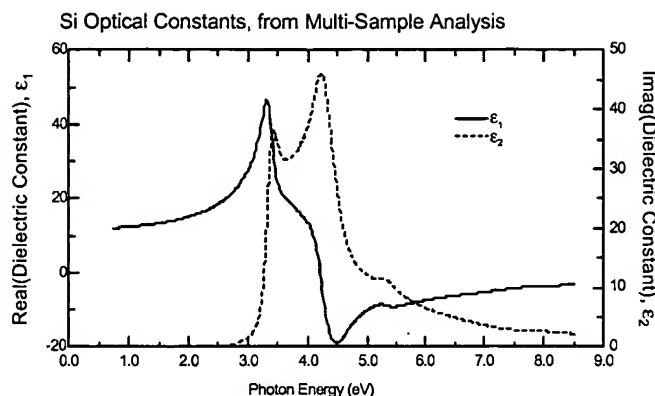


Figure 15. Si optical constants covering the NIR-VIS-UV-VUV spectral range (0.75 – 8.5 eV, or 146 – 1650 nm) extracted from a multi-sample VASE analysis of SiO<sub>2</sub> on Si wafers.

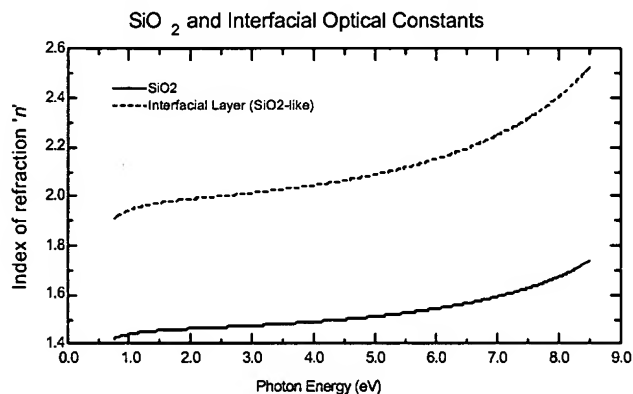


Figure 16. SiO<sub>2</sub> and Si/oxide interfacial optical constants covering the NIR-VIS-UV-VUV spectral range (0.75 – 8.5 eV, or 146 – 1650 nm) extracted from a multi-sample VASE analysis of SiO<sub>2</sub> on Si wafers.

### 3. BEYOND ISOTROPIC

Traditionally, most ellipsometric measurements have assumed an isotropic and non-depolarizing sample. While this assumption is indeed valid for most measurements, there are classes of samples which do exhibit anisotropic and/or depolarizing behavior. In these cases, it is not possible to adequately characterize the sample by a simple ellipsometric measurement of  $\Psi$  and  $\Delta$ . While the literature has addressed the theory of non-isotropic ellipsometric measurements<sup>37-40</sup>, recent advances in ellipsometric instrumentation<sup>7,14,41,42</sup> have made automated measurement of non-isotropic samples more practical, examples of which will be presented next.

#### 3.1. Generalized Variable Angle Spectroscopic Ellipsometry (g-VASE)

The interaction of polarized light with an isotropic sample can be represented by the Jones matrix formalism shown in equation (3). The diagonal nature of the Jones matrix

in this equation implies no sample-induced coupling between the p- and s- polarized modes.

$$\begin{bmatrix} P_{out} \\ S_{out} \end{bmatrix} = \begin{bmatrix} r_p & 0 \\ 0 & r_s \end{bmatrix} \cdot \begin{bmatrix} P_{in} \\ S_{in} \end{bmatrix} \quad (3)$$

The Jones matrix for a *general* sample is not necessarily diagonal, as shown in equation (4). For such a sample, three ellipsometric ratios can be defined; one possible notation for the general ellipsometric parameters<sup>43,44</sup> is listed in Equations (5a-5c). For an isotropic sample,  $A_{ps}=A_{sp}=0$ , and  $AnE$  reduces to the standard ellipsometric ratio given in equation (1). The three generalized ellipsometric ratios can be experimentally measured with standard ellipsometric instrumentation, however, special data acquisition schemes (which can be implemented in software) are usually required.

$$\begin{bmatrix} P_{out} \\ S_{out} \end{bmatrix} = \begin{bmatrix} r_{pp} & r_{sp} \\ r_{ps} & r_{ss} \end{bmatrix} \cdot \begin{bmatrix} P_{in} \\ S_{in} \end{bmatrix} \quad (4)$$

$$AnE = \tan(\Psi) \cdot e^{i\Delta} = \frac{r_{pp}}{r_{ss}} \quad (5a)$$

$$A_{ps} = \tan(\Psi_{ps}) \cdot e^{i\Delta_{ps}} = \frac{r_{ps}}{r_{pp}} \quad (5b)$$

$$A_{sp} = \tan(\Psi_{sp}) \cdot e^{i\Delta_{sp}} = \frac{r_{sp}}{r_{ss}} \quad (5c)$$

### 3.1.1. g-VASE Measurements of Anisotropic Plastics

Transmission mode g-VASE data acquired on a  $\approx 90 \mu\text{m}$  thick biaxially stretched plastic film (poly-ethyleneterephthalate, or PET) is shown in Figure 17. Note the incredible amount of structure in the plotted  $\Psi_{ps}$  quantity (which would be zero for an isotropic sample). This complex data set was also quantitatively analyzed (g-VASE data was calculated for the anisotropic optical model using a 4x4 matrix algorithm<sup>45</sup>) as evidenced by the data fits shown in Figure 18. The final result of the analysis was a determination of the three principal indices of refraction for the biaxial plastic (the index differences are plotted in Figure 19), which were found to be in excellent agreement with Abbe refractometer measurements, along with the azimuthal orientation of the film's optical axis. A detailed discussion of these results can be found in the literature<sup>44</sup>.

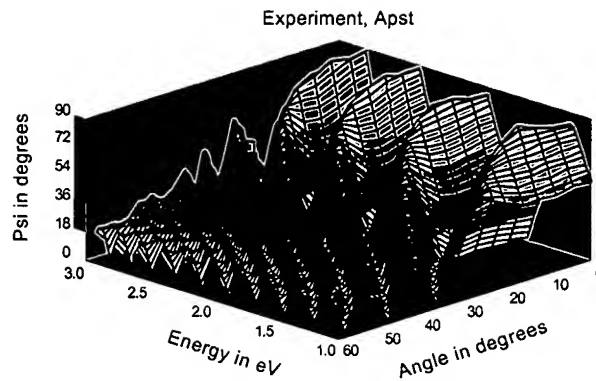


Figure 17. g-VASE data acquired on a biaxially stretched plastic film. The experimentally measured (in transmission) ellipsometric  $\Psi_{ps}$  value is plotted as a function of photon energy and angle of incidence.

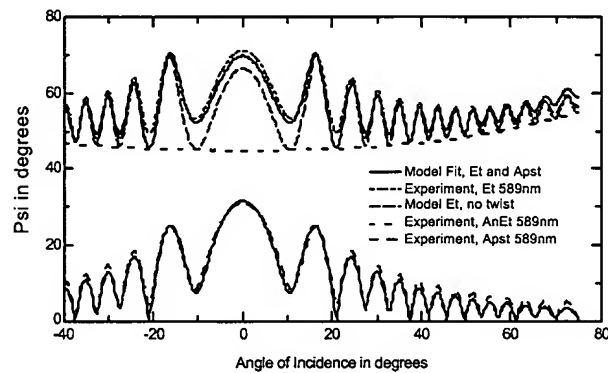


Figure 18. Quantitative analysis of g-VASE data acquired on a biaxially stretched plastic film, plotted at one wavelength vs. angle of incidence for clarity. The best model fit included a 'twist' in the orientation of the optical axis from the top to the bottom of the film.

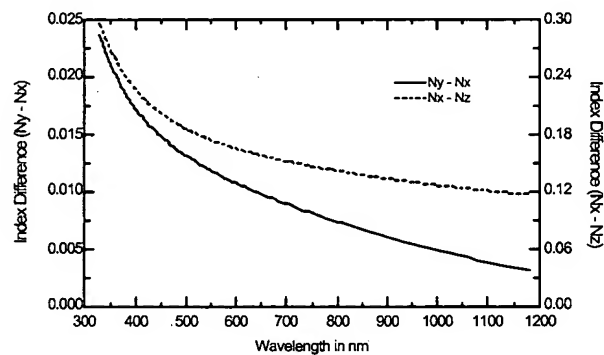


Figure 19. Difference of the principal indices of refraction, extracted from the analysis of the PET film g-VASE data shown in Figures 17 and 18.

### 3.1.2. Diode Array Rotating Compensator Ellipsometer g-SE Measurements

In addition to advantages discussed in section 1.1.2, the rotating compensator ellipsometer (RCE) configuration is also well suited for generalized ellipsometry measurements. Not only can the RCE accurately measure  $\Delta$  over the full  $0 - 360^\circ$  range, it also measures  $\Psi$  accurately over the full  $0 - 90^\circ$  range (RAE systems also lose sensitivity when  $\Psi$  approaches  $0^\circ$  or  $90^\circ$ ). The ability to accurately measure very small  $\Psi$  values is very useful when performing generalized ellipsometry measurements, as the 'off-diagonal' ellipsometric ratios  $A_{ps}$  and  $A_{sp}$  (and therefore  $\Psi_{ps}$  and  $\Psi_{sp}$ ) are zero and near-zero, for isotropic and slightly anisotropic samples respectively. A Diode Array Rotating Compensator Ellipsometer (DARCE) system can rapidly perform generalized spectroscopic ellipsometer (g-SE) measurements by acquiring data sets at analyzer azimuths of  $0^\circ$ ,  $45^\circ$ , and  $90^\circ$ , and algebraically transforming the three data sets into the notation shown in Equations (4-5). An example of DARCE g-SE measurements is shown in Figure 20. The acquisition of this data required only a few seconds; there should be many potential applications for the fast anisotropic material characterization capability provided by a DARCE g-SE measurements.

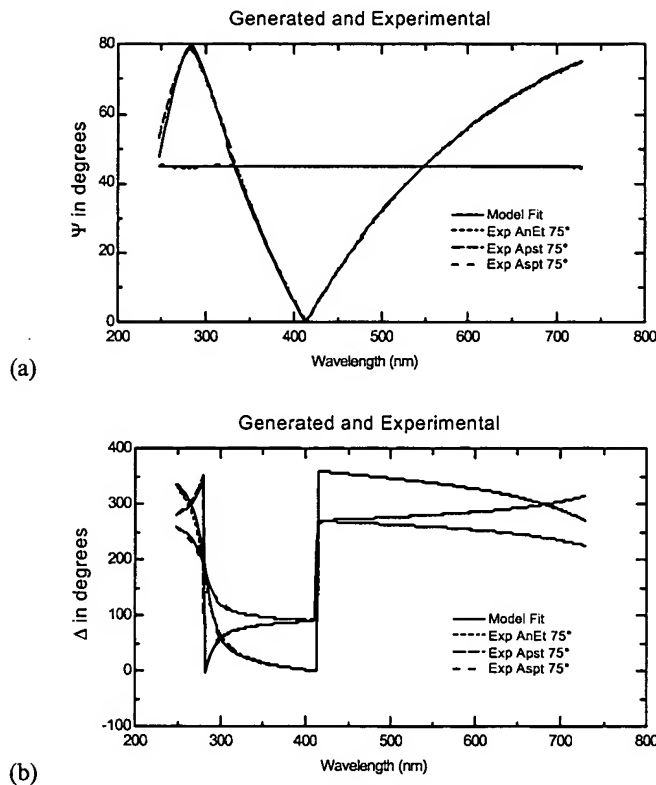


Figure 20. Generalized Spectroscopic Ellipsometric (g-SE) data acquired on a  $\text{MgF}_2$  Berek waveplate in transmission mode, using a Diode Array Rotating Compensator Ellipsometer (DARCE)<sup>14</sup>. The excellent model fit to the data required only two fit parameters: the plate tip and rotation angles.

### 3.2. Depolarization Measurements

Another implicit assumption in the traditional ellipsometry equation (1) is that the beam reflected from the sample is totally polarized. However, if the sample depolarizes the measurement beam, the ellipsometric parameters  $\Psi$  and  $\Delta$  are not well defined, and the measured ‘effective’  $\Psi$  and  $\Delta$  values will be dependent on the type of ellipsometer system used to acquire the data. To consider the case of a depolarizing sample requires a different formalism from the Jones matrix notation presented in the preceding section. A partially polarized beam can be quantified by a 4 element Stokes vector<sup>46</sup>, and a 16 element Mueller matrix then completely specifies the interaction of the beam with a sample (see Equation 6). The Mueller matrix for an isotropic sample is given in Equation 7. Note that the isotropic Mueller matrix elements denoted N, C, S are defined in terms of trigonometric functions of the ellipsometric parameters  $\Psi$  and  $\Delta$ . The quantity ‘P’, known as the degree of polarization, is defined in Equation 8 as the sum of the squares of N, C, and S; this quantity should be 1.0 for a non-depolarizing sample. If the sample depolarizes the measurement beam, the degree of polarization will be less than 1.0. Alternatively, the % depolarization can be reported, as also defined in equation 8. Even in the presence of depolarization, ellipsometric parameters  $\Psi$  and  $\Delta$  can be calculated which reduce to the traditional ellipsometric values in the case of no depolarization (Equation 9). Experimentally measuring the % depolarization (or equivalently, the degree of polarization ‘P’) requires a compensator-based ellipsometer configuration, as the RAE and RPE configurations can not directly measure beam depolarization effects (though their effect on the RAE or RPE ellipsometric data can still be correctly accounted for in the data analysis<sup>40</sup>).

$$\begin{bmatrix} S_1 \\ S_2 \\ S_3 \\ S_4 \end{bmatrix}_{out} = \begin{bmatrix} m_{11} & m_{12} & m_{13} & m_{14} \\ m_{21} & m_{22} & m_{23} & m_{24} \\ m_{31} & m_{32} & m_{33} & m_{34} \\ m_{41} & m_{42} & m_{43} & m_{44} \end{bmatrix} \cdot \begin{bmatrix} S_1 \\ S_2 \\ S_3 \\ S_4 \end{bmatrix}_{in} \quad (6)$$

$$M_{isotropic} = \begin{bmatrix} 1 & -N & 0 & 0 \\ -N & 1 & 0 & 0 \\ 0 & 0 & C & S \\ 0 & 0 & -S & C \end{bmatrix} \quad \begin{aligned} N &= \cos(2\Psi) \\ C &= \sin(2\Psi) \cdot \cos(\Delta) \\ S &= \sin(2\Psi) \cdot \sin(\Delta) \end{aligned} \quad (7)$$

$$P = N^2 + C^2 + S^2 \quad \% \text{ Depolarization} = 100 \times (1 - P) \quad (8)$$

$$\Psi = \frac{1}{2} \cdot \text{atan} \left( \frac{\sqrt{C^2 + S^2}}{N} \right) \quad \Delta = \text{atan} \left( \frac{S}{C} \right) \quad (9)$$

#### 3.2.1. Film Thickness Non-uniformity and Spectrometer Bandwidth

Two common sources of depolarization are film thickness non-uniformity and spectrometer bandwidth (for small spot focused beam ellipsometer systems, the angle



spread of the beam is another source of depolarization). As the ellipsometric beam spot size on the sample is relatively large (1 x 4 mm is typical), it is quite possible that the film thickness is not completely uniform in this area. In this case, the interaction of various partitions of the beam with films of slightly differing thicknesses could be represented by a collection of Mueller matrices, and the net interaction of the beam with the sample over the measurement area could be modeled by a weighted average of all the corresponding Mueller matrices. % depolarization and ellipsometric parameters can be calculated from this 'net' Mueller matrix, using Equations 8 and 9. Note that since the Mueller matrix corresponding to each beam partition is of the form given in Equation 7, the net Mueller matrix is also of this form; however, the % depolarization of the net Mueller matrix is not necessarily zero. Depolarization due to finite spectrometer bandwidth can also be understood in a similar fashion, in that the collected beam contains a range of wavelengths, and a net Mueller matrix can again be found by calculating the weighted average of Mueller matrices which characterize the sample interaction vs. wavelength. In both cases, the depolarization calculation can be numerically performed in software, given an appropriate weighting function. An example of these effects is shown in Figure 21, and other examples can be found in the literature<sup>47,48</sup>. Depolarization caused by the backside reflection of a transparent substrate is shown in Figure 4.

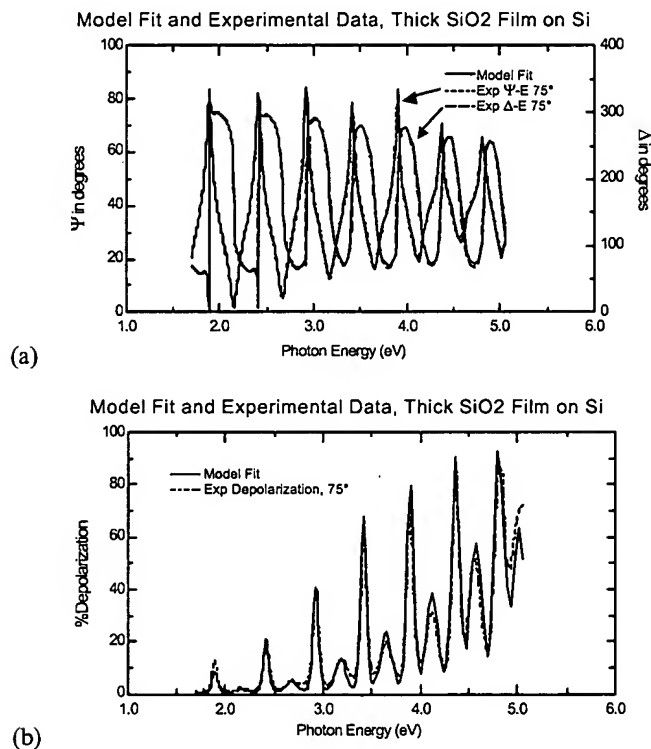


Figure 21. Spectroscopic ellipsometric (a) and depolarization (b) data acquired on a 10540Å SiO<sub>2</sub> film on Si by a DARCE instrument<sup>14</sup>. To fit the depolarization data, a spectrometer bandwidth of 7nm (assuming a Gaussian profile) and a film thickness non-uniformity of 0.44% were included in the optical model.

### 3.2.2. Patterned Samples

Patterned samples can also cause depolarization effects which can be readily measured and quantitatively analyzed. Actually, patterning can be simply treated as a case of film thickness non-uniformity with only a few discrete thickness values. Figure 22 shows a patterned sample in which the ellipsometric beam encompasses two regions of differing oxide thicknesses. Experimental data and the resulting model fits for such a sample are shown in Figure 23. In this analysis of this data, the native and thermal oxide thicknesses were determined ( $18.6 \pm 0.3 \text{ \AA}$  and  $998.2 \pm 0.5 \text{ \AA}$ ), along with the % patterned area (thermal oxide removed) covered by the measurement beam ( $67.5 \pm 0.1\%$ ). The patterned results were confirmed by measuring each region individually, which is also shown in the figures. As expected, the % depolarization is essentially zero for the unpatterned areas of the sample (the non-zero values below 300nm are due to stray light in the spectrometer). As patterned samples are commonplace in the manufacturing environment, the ability to quantitatively analyze data on patterned product wafers can be an enabling factor in the implementation of ellipsometric process monitoring and control (it is not desirable to dedicate wafer real estate to large metrology pads, and it is not always feasible to perform focused-beam ellipsometric measurements, for example, when performing *in situ* metrology). It should be noted that the analysis method described in this section is only valid for samples with patterning dimensions much larger than the wavelengths used in the ellipsometric measurement beam; however, an approach described by Maynard<sup>49</sup> may work in the very small pattern dimensions regime.

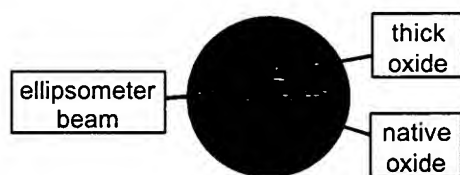
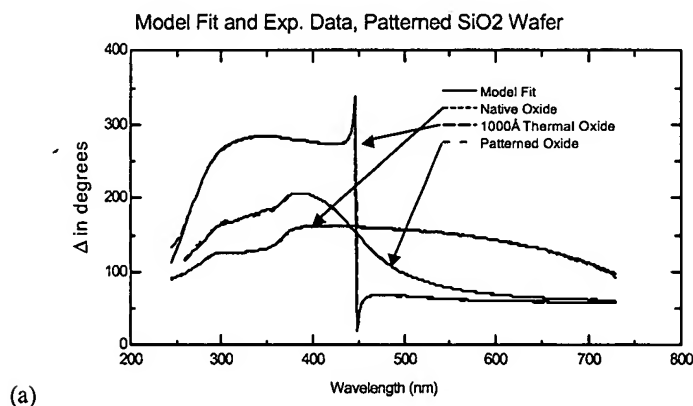


Figure 22. Schematic representation of the ellipsometric measurement of a patterned oxide sample, in which the beam overlaps native and thick oxide regions of the sample.



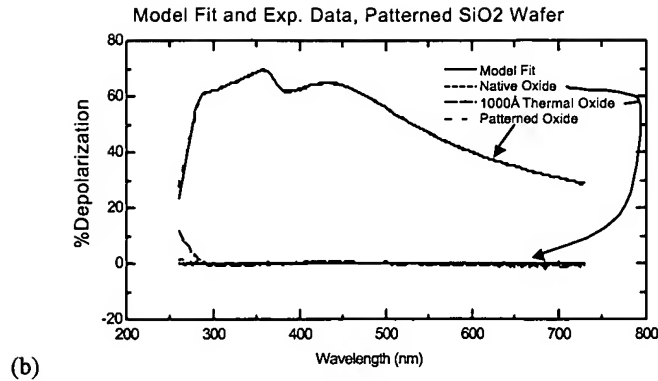


Figure 23. Spectroscopic ellipsometric (a) and depolarization (b) data acquired on a patterned  $\text{SiO}_2$  film on Si by a DARCE instrument<sup>14</sup> (data measured on unpatterned native and thermal oxide areas are also shown).

### 3.3. Mueller Matrix Measurements

The Mueller matrix shown in Equation 6 completely specifies the specular optical response of a general sample (which may be anisotropic, depolarizing, and/or cross polarizing) at a given wavelength. Recent instrumentation<sup>7,14,41,42</sup> is capable of performing spectroscopic measurements of all 16 (or some subset) of the Mueller matrix elements, an example of which is shown in Figure 24. Unfortunately, the current data analysis capabilities for such measurements are essentially limited to samples which have a Mueller matrix of the form shown in Equation 7 (or its anisotropic generalization<sup>50</sup>). Nevertheless, Mueller matrix measurements can still be used to observe (even though they may not be quantitatively modelable) the cross polarization and scattering effects which are induced by very rough samples. Mueller matrix measurements can also be used to confirm the ideality of a sample or optical element, that is, the off-diagonal blocks of matrix elements should be zero and the  $m_{22}$  element should be 1.0.

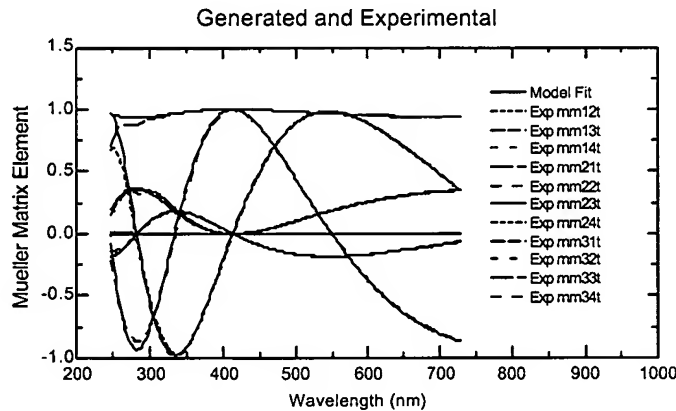


Figure 24. Mueller matrix measurement and data analysis for the  $\text{MgF}_2$  Berek waveplate which was also measured for Figure 20. The measurement was performed with a DARCE system<sup>14</sup>, which can measure 11 normalized (to  $m_{11}$ ) Mueller matrix elements (the bottom row of the Mueller matrix is not accessible, as the compensator was placed before the sample).

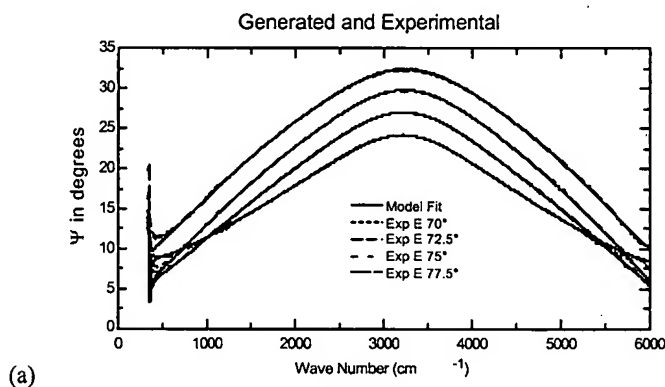
#### 4. EXTENDED SPECTRAL RANGES: FROM IR TO VUV

A strong motivation exists to measure material optical constants over increasingly broader spectral ranges. This section describes recent instrumentation advances which enable accurate measurement of ellipsometric data from the IR to VUV spectral ranges, along with examples of this powerful capability.

##### 4.1. VASE Measurements in the IR

Fourier Transform Infra Red (FTIR) spectroscopy is a well established diagnostic technique, and in theory the advantages of ellipsometry can be applied to FTIR by adding polarizing optics to an FTIR system<sup>51</sup>. In practice, it is very challenging to build an accurate FTIR ellipsometer system, due to the lack of ideal optical components (both polarizers and compensators) in the IR spectral range<sup>22</sup>. However, by implementing a sophisticated regression calibration procedure<sup>6</sup> to fully characterize the non-idealities of the optical elements, and incorporating a novel IR compensator design<sup>15</sup>, an accurate RCE FTIR system has been constructed<sup>12,13</sup>. This instrument can acquire VASE data over a 2 – 33  $\mu\text{m}$  spectral range, with an absolute ellipsometric accuracy shown in Figures 6 and 7.

Examples of IR VASE data are shown in Figures 25 - 28. In these examples, VASE measurements in the IR are used to determine the optical constants and thickness of an IR optical coating, the doping concentration<sup>12</sup> and oxide thickness of a Si substrate, and IR optical constants of glass and organic materials are shown to be highly sensitive to the bonding chemistry of the material. While all of the data analysis techniques used for NIR-VIS-UV VASE data can also be applied in the IR (note the excellent model fits in Figures 25 and 26), additional analysis techniques need to be developed to quantify the rich bonding and chemistry information contained in the spectra shown in Figures 27 and 28.



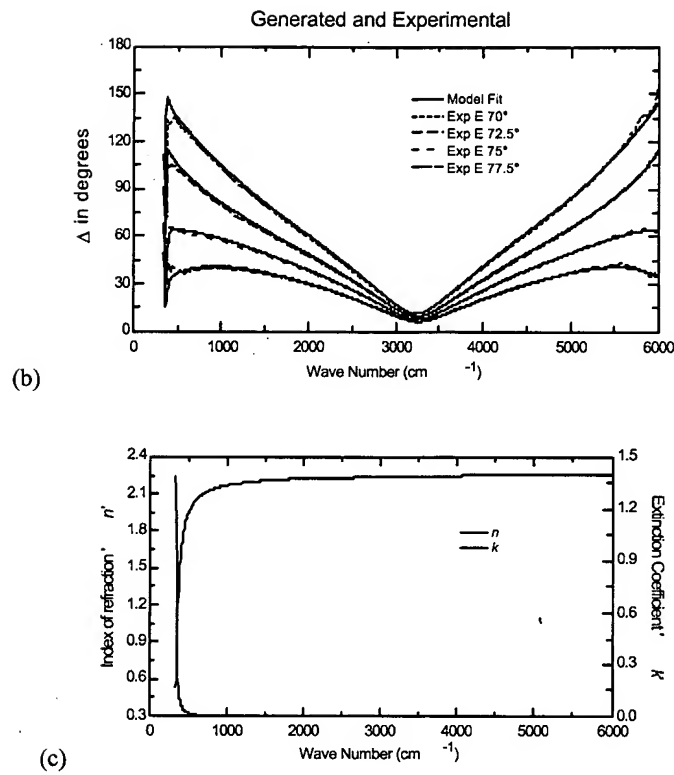
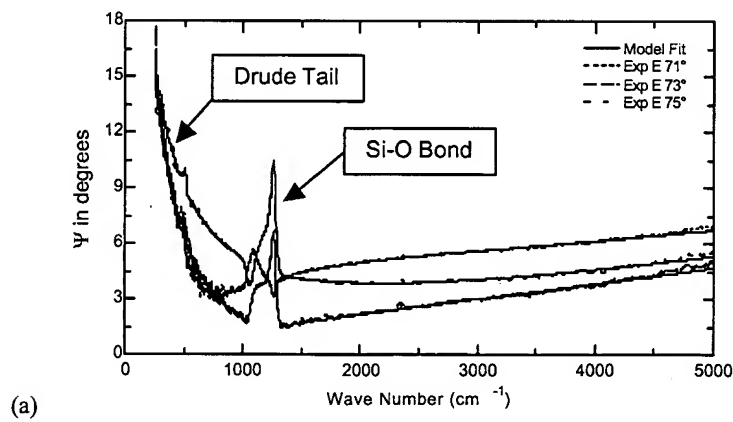


Figure 25. (a,b) IR-VASE data acquired on a 3792Å ZnS film deposited on Si. (c) resulting ZnS IR optical constants extracted from the analysis of this data.



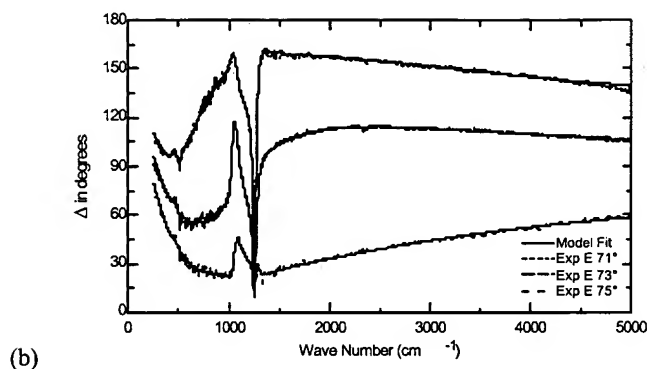


Figure 26. (a,b) IR-VASE data acquired and analyzed on a 268Å thermal oxide film on a doped Si substrate. Features due to the free carrier absorption (Drude tail) and the Si-O bond absorption are clearly seen in the data.

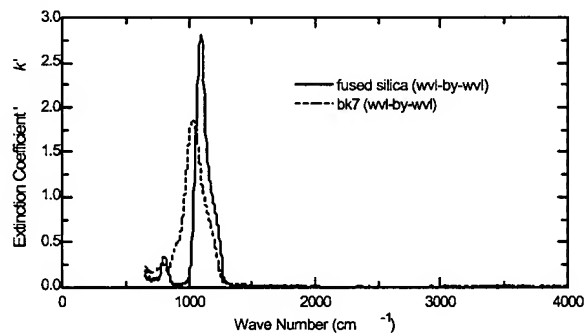


Figure 27. Extinction coefficient 'k' for bulk fused silica and BK7 glass extracted from IR-VASE data. In the visible spectral range, the optical constants for these materials are featureless and nearly the same. In IR range, the Si-O bond feature near 1000 cm<sup>-1</sup> clearly differentiates these two materials.

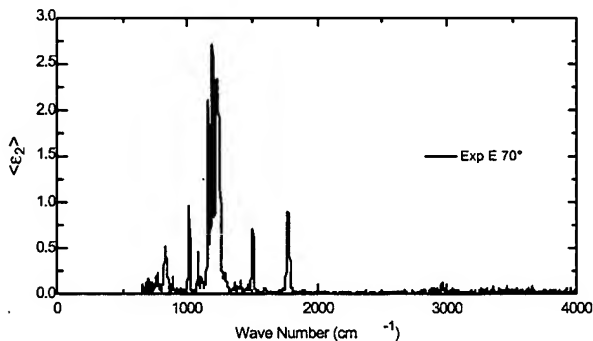


Figure 28. Imaginary part of the dielectric function,  $\epsilon_2$ , directly extracted from the IR-VASE measurement of a bulk polycarbonate sample. The RCE configuration of the instrument enabled the accurate measurement of the low  $\epsilon_2$  values in this spectral range, as the ellipsometric  $\Delta$  parameter is essentially zero for most of this data set. Note the abundance of sharp IR absorption bands, which is typical of most organic materials, and may be used to directly characterize the chemistry of the material.

## 4.2. VUV Ellipsometry

A RAE system equipped with an adjustable retarder<sup>7</sup> has been operated in the UV-VUV spectral range (4.2 – 8.5 eV, or 146 – 300 nm). To achieve operation in this spectral range, a deuterium lamp coupled with a scanning monochromator was used as a light source, along with MgF<sub>2</sub> optics. Examples of spectroscopic ellipsometric data acquired with this system are shown in Figure 29, and in section 2.2 of this paper. As the next targeted lithography line is 157nm, there is a tremendous demand for optical constant measurements in this VUV spectral range of materials used in Si-based semiconductor technology (especially photoresists), and of optical elements (and coatings) used in lithographic stepper equipment. Wide band-gap materials such as Al<sub>x</sub>Ga<sub>1-x</sub>N (which is used in blue LEDs and lasers) will also benefit from VASE characterization in the VUV spectral range<sup>53</sup>.

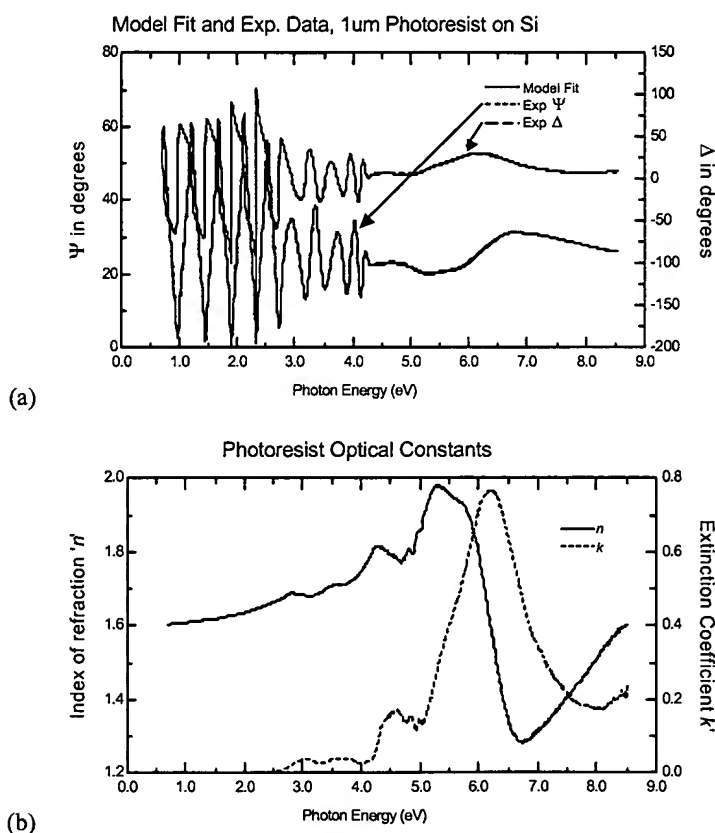


Figure 29. (a) UV-VUV spectroscopic ellipsometric data from a  $\approx 1 \mu\text{m}$  photoresist film on Si; NIV-VIS-UV data acquired on a different instrument is also appended to the curve. (b) Photoresist optical constants resulting from an analysis of the data, using the Si substrate optical constants shown in Figure 15.

## SUMMARY

Advanced instrumentation which can acquire extremely accurate VASE data, generalized ellipsometry data, depolarization and Mueller matrix data over a broad spectral range (IR to VUV) has greatly enhanced the material characterization capabilities of the VASE technique, as illustrated by the many applications in this paper. The accuracy of the measured data and the validity of the optical models used in the data analysis were confirmed by the near perfect data fits which were achieved in these applications. Powerful data analysis techniques such as GBPS parameterization and multi-sample analysis were also shown to be extremely useful in extracting material properties (optical constants and structural parameters) from the wide spectral range measurements.

## ACKNOWLEDGMENTS

The authors wish to thank the many sponsors who contributed to the development of the work presented here, including NASA, BMDO, the U.S. Army and Air Force, DARPA, and numerous corporations which supplied samples.

## REFERENCES

1. P.S. Hauge, "Recent developments in instrumentation in ellipsometry", *Surf. Sci.* 96, 108 (1980).
2. R.W. Collins, "Automatic rotating element ellipsometers: Calibration, Operation, and Real-time Applications", *Rev. Sci. Instrum.* 61, 2029 (1990).
3. J.M.M. de Nijs and A. van Silfhout, "Systematic and random errors in rotating-analyzer ellipsometry", *J. Opt. Soc. Am. A* 5, 773 (1988).
4. B. Drevillon, J. Perrin, R. Marbot, A. Violet, and J.L. Dalby, *Rev. Sci. Instrum.* 53, 969 (1982).
5. G.E. Jellison Jr. and F.A. Modine, "A two-channel polarization modulation ellipsometer", *Appl. Opt.* 29, 959 (1990).
6. B. Johs, "Regression calibration method for rotating element ellipsometers", *Thin Solid Films* 234, 395 (1993).
7. VASE system with AutoRetarder option, J.A. Woollam Co., Inc., Lincoln, NE USA.
8. US Patent #5,757,494, "System and method for improving data acquisition capability in spectroscopic ellipsometers".
9. R. Kleim, L. Kuntzler, and A. El Ghemmaz, "Systematic errors in rotating compensator ellipsometry", *J. Opt. Soc. Am. A* 11, 2550 (1994).
10. J. Lee, P.I. Rovira, I. An, and R.W. Collins, "Rotating compensator multichannel ellipsometry: applications for real time Stokes vector spectroscopy of thin film growth", *Rev. Sci. Instrum.* 69, 1800-1810 (1998).
11. J. Opsal, J. Fanton, J. Chen, J. Leng, L. Wei, C. Uhrich, M. Senko, C. Zaiser, D.E. Aspnes, "Broadband spectral operation of a rotating-compensator ellipsometer", *Thin Solid Films* 313-314, 58 (1998).
12. T.E. Tiwald, D.W. Thompson, J.A. Woollam, W. Paulson, and R. Hance, "Application of IR variable angle spectroscopic ellipsometry to the determination of free carrier concentration depth profiles", *Thin Solid Films* 313-314, 661 (1998).
13. IR-VASE system, J.A. Woollam Co., Inc., Lincoln, NE USA.
14. M-2000 ellipsometer system, J.A. Woollam Co., Inc., Lincoln, NE USA.
15. US Patent #5,706,212, "Infrared ellipsometer/polarimeter system, method of calibration, and use thereof".



16. US Patent #5,872,630, "Regression calibrated spectroscopic rotating compensator ellipsometer system with photo array detector".
17. R.W. Collins, I. An, H. Fujiwara, J. Lee, Y. Lu, J. Koh, and P.I. Rovira, "Advances in multichannel spectroscopic ellipsometry", *Thin Solid Films* 313-314, 18 (1998).
18. R.A. Synowicki, "Spectroscopic ellipsometry characterization of indium tin oxide film microstructure and optical constants", *Thin Solid Films* 313-314, 394 (1998).
19. T. Yasuda and D.E. Aspnes, "Optical-standard surfaces of single-crystal silicon for calibrating ellipsometers and reflectometers", *Applied Optics* 33, 7435 (1994).
20. G.E. Jellison Jr., "Examination of thin  $\text{SiO}_2$  films on Si using spectroscopic polarization modulation ellipsometry", *J. Appl. Phys.* 69, 7627 (1991).
21. C.M. Herzinger, B. Johs, W.A. McGahan, J.A. Woollam, and W. Paulson, "Ellipsometric determination of optical constants for silicon and thermally grown silicon dioxide via a multi-sample, multi-wavelength, multi-angle investigation", *J. Appl. Phys.* 83, 3323 (1998).
22. M. Luttmann, J-L Stehle, C. Defranoux, and J-P Piel, "High accuracy IR ellipsometer working with a Ge brewster angle reflection polarizer and grid analyzer", *Thin Solid Films* 313-314, 631 (1998).
23. G.E. Jellison Jr., "Data analysis for spectroscopic ellipsometry", *Thin Solid Films* 234, 416 (1993).
24. F. Wooten, *Optical Properties of Solids*, Academic press, New York, 1972.
25. F. Terry Jr., "A modified harmonic oscillator approximation scheme for the dielectric constants of  $\text{AlGa}_{1-x}\text{As}$ ", *J. Appl. Phys.* 70, 409 (1991).
26. G.E. Jellison Jr. and F.A. Modine, "Parameterization of the optical functions of amorphous materials in the interband region", *Appl. Phys. Lett.* 69, 371 (1996).
27. C.C. Kim, J.W. Garland, H. Abad, and P.M. Raccach, "Modeling the optical dielectric function of semiconductors: extension of the critical-point parabolic-band approximation", *Phys. Rev. B* 45, 11749 (1992).
28. S. Zollner, "Model dielectric function for native oxides on compound semiconductors", *Appl. Phys. Lett.* 63, 2523 (1993).
29. J. Leng, J. Opsal, H. Chu, M. Senko, and D.E. Aspnes, "Analytic representations of the dielectric functions of materials for device and structural modeling", *Thin Solid Films* 313-314, 132 (1998).
30. US Patent #5,796,983, "Dielectric function parametric model, and method of use".
31. B. Johs, C.M. Herzinger, J.H. Dinan, A. Cornfeld, and J.D. Benson, "Development of a parametric optical constant model for  $\text{Hg}_{1-x}\text{Cd}_x\text{Te}$  for control of composition by spectroscopic ellipsometry during MBE growth.
32. H.G. Tompkins, *A User's Guide to Ellipsometry*, Academic Press (1993).
33. C.M. Herzinger, H. Yao, P.G. Synder, F.G. Celii, Y.-C. Kao, B. Johs, and J.A. Woollam, "Determination of AlAs optical constants by variable angle spectroscopic ellipsometry and an multisample analysis", *J. Appl. Phys.* 77, 4677 (1995).
34. W.A. McGahan, B. Johs, and J.A. Woollam, "Techniques for ellipsometric measurement of the thickness and optical constants of thin absorbing films", *Thin Solid Films* 234, 443 (1993).
35. D.E. Aspnes and A.A. Studna, *Phys. Rev. B* 26, 7466 (1983).
36. G.E. Jellison Jr., *Opt. Mater.* 1, 41 (1992).
37. R.M.A. Azzam and N.M. Bashara, "Generalized ellipsometry for surfaces with directional preference: application to diffraction gratings", *J. Opt. Soc. Am.* 62, 883 (1972).
38. M. Schubert, "Generalized ellipsometry and complex optical systems", *Thin Solid Films* 313-314, 323 (1998).
39. A R\*seler, "Problem of polarization degree in spectroscopic photometric ellipsometry (polarimetry)", *J. Opt. Soc. Am. A* 9, 1124 (1992).
40. K. Forcht, A. Gombert, R. Joerger, M. K\*hl, "Incoherent superposition in ellipsometric measurements", *Thin Solid Films* 302, 43 (1997).
41. R.W. Collins and J. Koh, "Dual rotating compensator multichannel ellipsometer: instrument design for real time Mueller matrix spectroscopy of surfaces and films" *J. Opt. Soc. Am. A* 16 (in press, August 1999).

42. G.E. Jellison Jr., F.A. Modine, and L.A. Boatner, "The measurement of the optical functions of uniaxial materials using two-modulator generalized ellipsometry: Rutile ( $\text{TiO}_2$ )", *Opt. Lett.* 22, 1808 (1997).
43. M. Schubert, B. Rheinlander, J.A. Woollam, B. Johs, and C.M. Herzinger, "Extension of rotating-analyzer ellipsometry to generalized ellipsometry: determination of the dielectric function tensor from uniaxial  $\text{TiO}_2$ ", *J. Opt. Soc. Amer. A* 13, 876 (1996).
44. J.F. Elman, J. Greener, C.M. Herzinger, and B. Johs, "Characterization of biaxially-stretched plastic films by generalized ellipsometry", *Thin Solid Films* 313-314, 814 (1998).
45. M. Schubert, "Polarization-dependent optical parameters of arbitrarily anisotropic homogeneous layered systems", *Phys. Rev. B* 53, 4265 (1996).
46. R.M.A. Azzam, and N.M. Bashara, Ellipsometry and Polarized Light, North Holland Press, Amsterdam 1977, Second edition 1987.
47. G.E. Jellison Jr. and J.W. McCamy, "Sample depolarization effects from thin films of ZnS on GaAs as measured by spectroscopic ellipsometry", *Appl. Phys. Lett.* 61, 512 (1992).
48. U. Richter, "Application of the degree of polarization to film thickness gradients", *Thin Solid Films* 313-314, 102 (1998).
49. H.L. Maynard, N. Layadi, J.T.C. Lee, "Plasma etching of submicron devices : in situ monitoring and control by multi-wavelength ellipsometry", *Thin Solid Films* 313-314, 398 (1998).
50. G.E. Jellison Jr., "Spectroscopic ellipsometry data analysis: measured versus calculated quantities", *Thin Solid Films* 313-314, 33 (1998).
51. A. Rastels, Infrared Spectroscopic Ellipsometry, Akademie-Verlag, Berlin, 1990.
52. C.M. Herzinger, B. Johs, W.A. McGahan, W. Paulson, "A multi-sample, multi-wavelength, multi-angle investigation of the interface layer between silicon and thermally grown silicon dioxide", *Thin Solid Films* 313-314, 281 (1998).
53. T. Wethkamp, K. Wilmers, N. Esser, W. Richter, O. Ambacher, H. Angerer, G. Jungk, R.L. Johnson, M. Cardona, "Spectroscopic ellipsometry measurements of  $\text{Al}_x\text{Ga}_{1-x}\text{N}$  in the energy range 3-25 eV", *Thin Solid Films* 313-314, 745 (1998).

# Optical characterization in the vacuum ultraviolet with Variable Angle Spectroscopic Ellipsometry: 157 nm and below

James N. Hilfiker<sup>a</sup>, Bhanwar Singh<sup>b</sup>, R.A. Synowicki<sup>a</sup>, and C. L. Bungay<sup>a</sup>

<sup>a</sup>J. A. Woollam Co., Inc., 645 M Street, Lincoln, NE 68508

<sup>b</sup>AMD Corporation, One AMD Place, Sunnyvale, CA 94086

## ABSTRACT

As device feature sizes shrink below 0.18  $\mu\text{m}$ , shorter wavelength exposure tools are being investigated to meet the requirements for higher resolution. Understanding the optical properties of thin films and substrate materials at short wavelengths (193 nm, 157 nm, and shorter) will be necessary to develop the lithographic process. Variable Angle Spectroscopic Ellipsometry (VASE) offers nondestructive and precise measurement of thin film thickness and refractive index in the wavelength range from 146 nm to 1700 nm.<sup>1</sup> VASE measurements provide a complete description of the thin film optical properties, which can be used to track process changes or variations in sample structure. Recent hardware innovations have extended VASE into the vacuum ultraviolet to meet lithography requirements at 157 nm.<sup>2</sup>

**Keywords:** 157nm lithography, Spectroscopic Ellipsometry, VASE, Thin Film Characterization, Refractive Index, Vacuum Ultraviolet Metrology

## 1. INTRODUCTION

Thin film characterization is the principal application of VASE. It can measure film thickness and the refractive index over a wide spectral range. The refractive index is an important property for thin films involved in lithography, because it describes how light of a given wavelength will interact with the material. VASE is used to characterize photoresists, antireflective coatings, masks, pellicles, and other lithography-oriented thin films.<sup>3-6</sup>

Ellipsometers reflect polarized light from a thin film, multilayer, or bulk material and detect the change in polarization introduced by the sample structure. The measurement is expressed as psi ( $\psi$ ) and delta ( $\Delta$ ), which are related to the Fresnel reflection coefficients by:<sup>7</sup>

$$\rho = \tan(\psi)e^{i\Delta} = \frac{R_p}{R_s} \quad (1)$$

where  $p$ - and  $s$ - refer to directions parallel and perpendicular to the plane of incidence, respectively. There are two independent parameters ( $\psi$  and  $\Delta$ ) for each measurement, compared to a single parameter ( $R$ ) from reflectometry. Two parameters can allow the determination of more material properties, with the addition of tighter constraints on the results. Both terms measured in ellipsometry relate to a *ratio* of two values; which make ellipsometry measurements insensitive to fluctuating light intensity, electronic drift, or scattered light loss.<sup>8</sup> In addition, the phase quantity ' $\Delta$ ' provides excellent sensitivity to the presence of very thin films. For these reasons, ellipsometers can be very accurate and highly reproducible.

We will discuss the development of a VUV ellipsometer. Features of this instrument, which impact the VUV measurements, are presented. Advantages of the VASE technique are reviewed, including a wide spectral range and variable angle of incidence. Finally, we present results from a variety of thin films being investigated for lithography at 157 nm. Both single and multilayer structures were measured, consisting of dielectric, semiconductor, and metal thin films. Thin film refractive index values are presented to show the variation of material properties in the vacuum ultraviolet.

## 2. ELLIPSOMETER DEVELOPMENT

Ellipsometry measurements in the VUV were first demonstrated in 1970.<sup>9</sup> These early ellipsometers combined a UHV chamber and Synchrotron radiation for the light source to achieve measurements in the VUV. Unfortunately, this arrangement is not practical for widespread use. Commercial ellipsometers are available over a wide spectral range, but were previously limited by ambient air absorption to wavelengths above 190 nm. The requirement to optically characterize materials at 157 nm has motivated the rapid development of a commercially available VUV ellipsometer.

The J.A. Woollam Company has developed an ellipsometer for the VUV, which covers wavelengths from below 146 nm to 1700 nm and an angle range from 25° to 90°. It is based on the rotating analyzer VASE<sup>®</sup> instrument that covers the 190 nm to 1700nm spectral range. It also incorporates the same computer-controlled MgF<sub>2</sub> Berek waveplate as a compensator to improve the ellipsometric  $\Delta$  measurement accuracy. The entire system is purged with dry nitrogen gas to avoid absorption of VUV light by ambient oxygen and water vapor. Light from both a Xenon and Deuterium lamp passes through a double-chamber Czerny-Turner type monochromator to provide wavelength selection and stray-light rejection. Computer-controlled slit widths can adjust the bandwidth to insure adequate spectral resolution of optical features in the data. A photomultiplier tube is utilized for signal detection in the ultraviolet, with a stacked Si/InGaAs photodiode detector for longer wavelengths. As shown in Figure 1, the VUV-VASE<sup>™</sup> also contains a sample load cell to optimize sample exchange. This design prevents ambient exposure to a majority of the optical path – the sample-load area is purged independently after the sample is loaded. In this manner, the oxygen and water vapor levels can be reduced for good signal-to-noise within minutes of sample exchange.

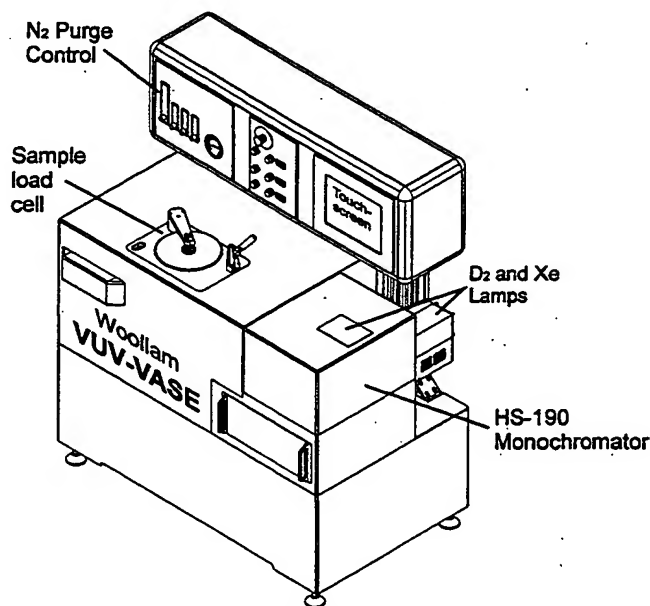


Fig 1. Schematic diagram of the VUV-VASE<sup>™</sup> used for measurements from 146 nm to 1700 nm.

### 2.1. Wide spectral range

The spectral range of an ellipsometer is its most important feature, as it determines the possible applications. For lithography films, it is important to measure the material characteristics at the exposure wavelength. However, other material properties may require a different spectral range. For instance, optical measurements in the transparent spectral range (where film is not absorbing) can precisely determine the film thickness. Other microstructural properties, such as composition, degree of crystallinity, and carrier concentration also require a specific spectral range to investigate.

The data shown in Figure 2 were measured on a sample of *Polysilicon / SiO<sub>2</sub> / Si* over the full range from 142 nm to 1700 nm (0.73 eV to 8.75eV). This wide spectral range provides information to characterize the entire film stack: SiO<sub>2</sub>

The silicon optical constants were determined using the same approach as Herzinger<sup>14</sup>. It involves simultaneously analyzing measurements from multiple samples consisting of the same materials. This method of "multi-sample analysis" has been shown to successfully enhance the information content about a set of samples.<sup>15</sup>

Another important method used to study silicon was the incorporation of a parametric dispersion model to describe the refractive index as a function of wavelength. This results in a much smaller set of free parameters than allowing the optical constants at each wavelength to be independent. Many different dispersion relationships have been applied to the analysis of VASE data; including Cauchy, Sellmeier, Tauc-Lorentz<sup>16</sup>, and more. We chose to use the parametric dispersion relationship developed by Herzinger and Johs.<sup>17</sup> This model offers many advantages over other dispersion relationships, although it does not try to directly capture the underlying physics of the material dielectric function: 1) it maintains Kramers-Kronig consistency, 2) flexibility to describe any material - dielectrics, semiconductors, metals,... 3) allows complete transparency below the fundamental bandgap, 4)  $\epsilon_2$  remains strictly positive, and 5) it can describe the subtle features which are often not adequately described by first principles physics-based models.

### 3.1 Metals

Metals are an integral part of microelectronic devices. These films are typically thick enough (>100nm) to be considered optically opaque because metals exhibit large absorption. For opaque films, the light cannot penetrate to the underlying interface and back to the surface. This removes the possibility of optically measuring the thickness, however it simplifies the data analysis of the metal surface. If the surface effects from oxide or roughness are negligible, then the measured ellipsometric  $\psi$  and  $\Delta$  can be directly inverted into the material 'pseudo-optical' constants. This transformation is given as:

$$\langle \epsilon \rangle = \langle \epsilon_1 \rangle + i \langle \epsilon_2 \rangle = \langle \tilde{n} \rangle^2 = (\langle n \rangle + i \langle k \rangle)^2 = \sin(\phi)^2 \cdot \left[ 1 + \tan(\phi)^2 \cdot \left( \frac{1 - \rho}{1 + \rho} \right)^2 \right] \quad (2)$$

where ' $\phi$ ' is the angle of incidence, ' $\rho$ ' is the complex ellipsometric ratio defined in Equation 1, ' $\epsilon$ ' is the dielectric function and the ' $\langle \rangle$ ' brackets represent a 'pseudo' parameter.

A thick layer of AlSiCu was measured with the VUV-VASE and analyzed via Equation 2 to determine pseudo-refractive index values. Figure 5 presents the experimental data and corresponding fit assuming a bulk sample. The graph provides pseudo-optical constants over the spectral range from 0.73 eV to 8.73 eV (142 nm to 1700 nm), which will be correct within the assumption that an oxidized or rough surface has insignificant effect on the measurement.

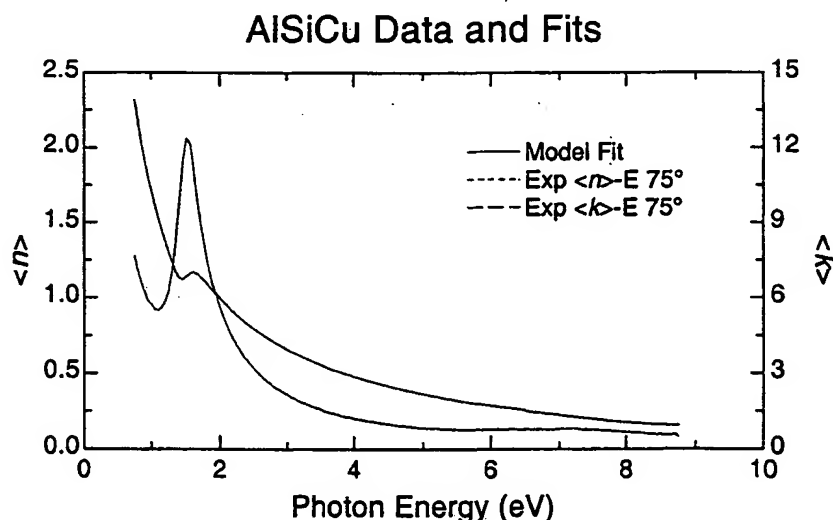


Fig 5. Experimental data and corresponding fit for an optically opaque layer of AlSiCu. The data are directly inverted at each wavelength using Equation 2 to determine pseudo-optical constants shown here.

There are a few applications which require a *thin* metallic layer. In this case, the light beam can probe through the film and determine the film thickness. It has been shown that ellipsometric characterization of a thin absorbing layer is enhanced by the presence of a thick underlying dielectric.<sup>18</sup> The underlying dielectric introduces a significant change in path length for different angles of incidence. This application *requires* multiple angles of incidence to separate the absorbing layer thickness from the layer refractive index. Titanium nitride layers have been characterized using this method. Figure 6 below shows the optical constants for a TiN film over the entire spectral range of the VUV-VASE.

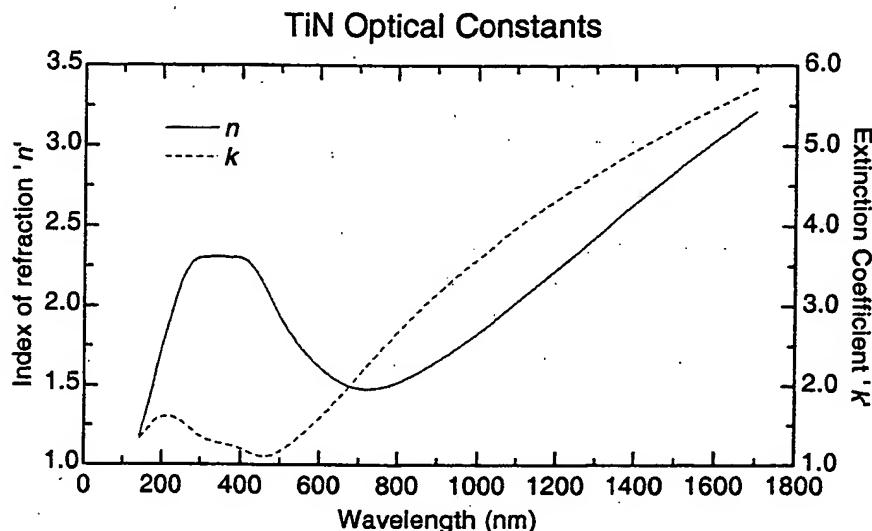


Fig 6. Refractive index of a TiN layer measured with VASE from 142 nm to 1700 nm.

### 3.2 Masks, Pellicles

VASE measurements have been used to develop photomask materials. Attenuated phase-shift masks can enable smaller features, but complex material structures are often required to produce the required properties. Index graded materials have been shown to produce the desired effects and VASE was successfully demonstrated for characterizing their optical properties.<sup>19,20</sup>

Pellicle materials are also optically characterized with VASE. Ultratransparent films are being developed at 157 nm to achieve the transmission requirements of pellicles.<sup>21</sup> The VASE measurements of fluoropolymer films being developed as potential pellicles has shown good agreement with absorbance measurements.

### 3.3 Photoresists

The materials used as photoresists will also require significant development for new lithography wavelengths. VASE is used to determine film thickness and refractive index of resists.<sup>3,4,13</sup> Typical resist materials are transparent in the visible and NIR. A simple dispersion layer, such as the Cauchy or Sellmeier models, can be used in the transparent range to find the index of refraction 'n' and the film thickness. If the model accurately describes the sample in this transparent region, then the layer thicknesses can be 'fixed', as they are not dependent on wavelength. This reduces the number of unknown 'free' parameters for the short wavelength analysis. At short wavelengths, where the film becomes absorbing, there are two remaining parameters – index of refraction 'n' and extinction coefficient 'k'. A wavelength-by-wavelength analysis will suffice to directly invert the model from  $\psi$  and  $\Delta$  to the two remaining unknowns – n and k. This analysis technique was used on the experimental data from a photoresist (AZ@AX1000P) shown in Figure 7. Measurements were taken over the entire spectra range, but are shown only for the short wavelengths. The resulting optical constants determined for this layer are provided in Figure 8.

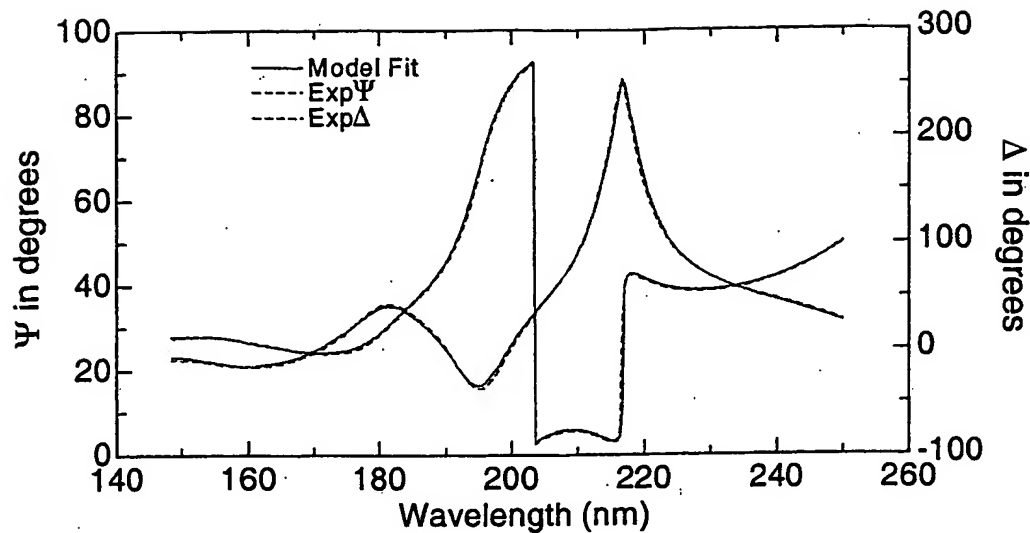


Fig 7. Experimental data and corresponding fits for a Photoresist layer on silicon. Data were measured over the entire spectral range from VUV to NIR, but are shown only for short wavelengths.

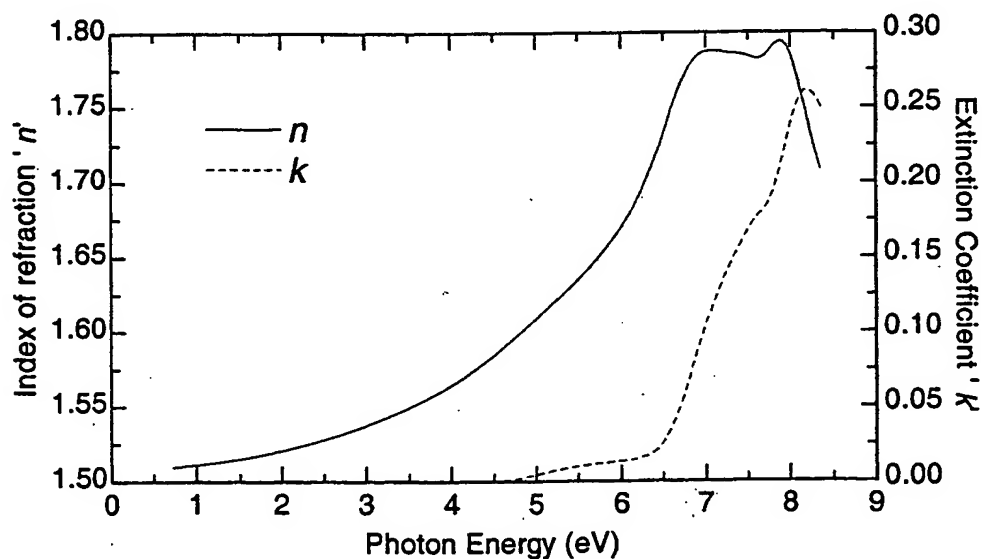


Fig 8. Optical constants for a Photoresist, measured using VASE over the spectral range from 146 nm to 1700 nm (0.73 eV to 8.5 eV).

### 3.4 AR Coatings

The lithography process often necessitates the use of AR coatings to optimize the process. The success of these films depends their optical properties. VASE is used to determine the film thickness and refractive index. It can also be used to study process variation. For instance, the change in refractive index can be determined as a function of bake conditions.<sup>12</sup> Other films, such as silicon oxynitride, offer a range of optical properties depending on deposition. This variability in refractive index is beneficial when used as an AR coating because its refractive index can be 'tuned' to meet a given application. We have measured a series of different silicon oxynitride films, which represent a range of properties. Both the index of refraction and extinction coefficient for these three films are shown in Figure 9.

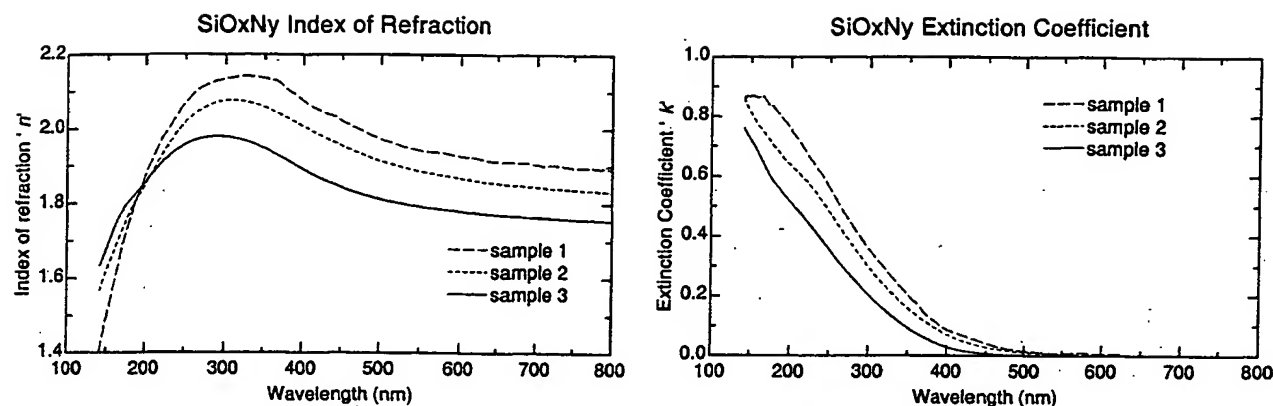


Fig 9. Index of refraction and extinction coefficient for three silicon oxynitride films from varying process conditions.

### 3.5 Optical Coatings

In addition to the films directly involved in the lithography steps, there will be many optical elements that can be enhanced with proper optical coatings. The merit of these coatings will depend on their refractive index, which can be measured with VASE. Most films investigated for use at 157 nm are deposited on  $\text{CaF}_2$  or BK7 substrates. It is advantageous to use the AutoRetarder when dealing with transparent substrates. First, the transparent substrate will introduce incoherent backside reflections, which can be quantified with the AutoRetarder measurement. Second, the Brewster condition for transparent substrates is very sharp. The AutoRetarder allows precise measurements away from the Brewster condition, where other ellipsometers have a difficult time with measurements. Fluoride films are popular candidates for short wavelength coatings because of their transparency. The refractive index for a series of fluorides have been measured and are provided in the table of results presented in the conclusion

## 4. CONCLUSIONS

Variable Angle Spectroscopic Ellipsometry (VASE) can be used to measure the film thickness and refractive index for a variety of materials used in lithography applications. A commercial ellipsometer has been developed to provide characterization into the VUV, which covers all of the current lithography lines: 248nm, 193nm, 157nm. A range of different thin films have been measured with this instrument to provide refractive index measurements. Table 2 provides the refractive index at 193 nm and 157 nm for many of the materials that were measured.

Material	n (193 nm)	k (193 nm)	n (157 nm)	k (157 nm)
Silicon (crystalline)	0.89	2.67	0.66	2.03
Silicon (polycrystalline)	1.23	2.72	0.89	2.08
$\text{SiO}_2$ (thermal)	1.573		1.676	
AlSiCu	0.130	1.568	0.116	1.111
TiN	1.662	1.593	1.313	1.402
SiON (film 1)	1.835	0.784	1.562	0.865
SiON (film 2)	1.827	0.657	1.661	0.781
SiON (film 3)	1.840	0.537	1.721	0.691
$\text{MgF}_2$	1.44		1.48	
$\text{LaF}_3$	1.72		1.83	

## ACKNOWLEDGMENTS

The authors from Woollam Company would like to thank Roger French, Ralph Dammell, Jeff Byers, and Pat Gabella for technical discussions. Their technical experience was greatly appreciated.



## REFERENCES

1. J. A. Woollam, B. Johs, C. M. Herzinger, J. Hilfiker, R. Synowicki, and C. L. Bungay, "Overview of Variable Angle Spectroscopic Ellipsometry (VASE), Part I: Basic Theory and Typical Applications," *SPIE Vol. CR72*, pp. 3-28, 1999.
2. B. Johs, J. A. Woollam, C. M. Herzinger, J. Hilfiker, R. Synowicki, and C. L. Bungay, "Overview of Variable Angle Spectroscopic Ellipsometry (VASE), Part II: Advanced Applications," *SPIE Vol. CR72*, pp. 29-58, 1999.
3. R. A. Synowicki, J. N. Hilfiker, R. R. Dammel, and C. L. Henderson, "Refractive Index Measurements of Photoresist and Antireflective Coatings with Variable Angle Spectroscopic Ellipsometry," *SPIE Vol. 3332*, pp. 384-390, 1998.
4. J. N. Hilfiker, R. Carpio, R. A. Synowicki, and J. A. Woollam, "Metrology Applications in Lithography with Variable Angle Spectroscopic Ellipsometry," *Characterization and Metrology for ULSI Technology - AIP Proc. 449*, ed. D. Seiler, et al. pp. 543-547, 1998.
5. J. N. Hilfiker and R. A. Synowicki, "Employing Spectroscopic Ellipsometry for Lithography Applications," *Semiconductor Fabtech*, Edition 5, pp. 189-194, 1996.
6. J. N. Hilfiker, C. Bungay, R. Synowicki, T. Tiwald, M. Liphardt, "Spectroscopic Ellipsometry in the Vacuum Ultraviolet: 157nm and below," *Future Fab International*, Edition 8, pp. 243-247, 1999.
7. R. M. A. Azzam and N.M. Bashara, *Ellipsometry and Polarized Light*, North Holland Press, Amsterdam, 1987.
8. D. E. Aspnes, "The Accurate Determination of Optical Properties by Ellipsometry," in *Handbook of Optical Constants of Solids*, ed. E. D. Palik, Academic Press, San Diego, p. 91, 1998.
9. J. Barth, R. L. Johnson, and M. Cardona, "Spectroscopic Ellipsometry in the 6-35eV Region," *Handbook of Optical Constants of Solids II*, ed. Palik, Academic Press, San Diego, pp. 213-246, 1998.
10. W. A. McGahan, B. R. Spady, B. D. Johs, O. Laparra, "Optical Characterization of Polycrystalline Silicon Thin Films," *SPIE Proc. Int. Symp. on Microlithography*, 1996.
11. US Patent #5,757,494, "System and method for improving data acquisition capability in spectroscopic ellipsometers."
12. R. R. Dammel, J. Sagan, and R. A. Synowicki, "Dependence of Optical Constants of AZ@BARLi™ Bottom Coating on Bake Conditions," *SPIE Vol. 3049*, pp. 963-973, 1997.
13. C. L. Henderson, C. G. Willson, R. R. Dammel, and R. A. Synowicki, "Bleaching-Induced Changes in the Dispersion Curves of DNQ Photoresists," *SPIE Vol. 3049*, pp. 585-595, 1997.
14. C. M. Herzinger, B. Johs, W. A. McGahan, J. A. Woollam, and W. Paulson, "Ellipsometric determination of optical constants for silicon and thermally grown silicon dioxide via a multi-sample, multi-wavelength, multi-angle investigation," *J. Appl. Phys.* **83** (6), pp. 3323-3336, 1998.
15. C. M. Herzinger, H. Yao, P. G. Snyder, F. G. Celii, Y. C. Kao, B. Johs, and J. A. Woollam, "Determination of AlAs optical constants by variable angle spectroscopic ellipsometry and a multisample analysis," *J. Appl. Phys.* **77** (9), pp. 4677-4687, 1995.
16. G. E. Jellison Jr. and F. A. Modine, "Parameterization of the optical functions of amorphous materials in the interband region", *Appl. Phys. Lett.* **69**, pp. 371-373, 1996.
17. US Patent #5,796,983, "Dielectric function parametric model, and method of use".
18. W. A. McGahan, B. Johs, and J. A. Woollam, "Techniques for ellipsometric measurement of the thickness and optical constants of thin absorbing films," *Thin Solid Films*, **234**, pp. 443-446, 1993.
19. F. D. Kalk et al., "Attenuated phase-shifting photomasks fabricated from Cr-based embedded shifter blanks", *Proc. SPIE*, 2254.
20. US Patents #5,393,465 and #5,415,953 (DuPont).
21. R. H. French, R. C. Wheland, D. J. Jones, J. N. Hilfiker, R. A. Synowicki, R. C. Zumsteg, J. Feldman, A. E. Feiring, "Fluoropolymers for 157nm Lithography: Optical properties from VUV Absorbance and Ellipsometry Measurements," submitted SPIE Microlithography 2000.

# A New Purged UV Spectroscopic Ellipsometer to characterize thin films and multilayers at 157nm

Pierre Boher\*, Jean Philippe Piel, Patrick Evrard,  
Christophe Defranoux, Marta Espinosa and Jean Louis Stehle  
SOPRA S.A., 26 rue Pierre Joigneaux, 92270 Bois Colombes, France.

## ABSTRACT

Spectroscopic ellipsometry is one of the more important tools for thin film metrology. It is now intensively used in microelectronics and especially for the microlithographic applications. Instrumentation for the next generation of UV lithography at 157nm requires special optical setup since oxygen and water are extremely absorbing below 190nm. The ellipsometer discussed in this paper works into a purged glove box to reduce the oxygen and water contamination in the part per million range. The optical setup has been especially studied for microlithographic applications with a premonochromator in the polariser arm to avoid resist photobleaching. Technical details of the system and measurements results on substrates and thin films are reported hereafter. Results are compared to those obtained with more standard ellipsometers and correlated to other results obtained with grazing x-ray reflectance technique.

Keywords: Spectroscopic Ellipsometry, 157nm, UV lithography

## 1. INTRODUCTION

Recently, there has been increasing interest in using 157nm laser sources in projection lithography as successors to 193nm based systems. This would follow the historical trends in the microelectronic industry where wavelength reduction is used to improve feature resolution. At 248 and 193nm, spectroscopic ellipsometry has shown to be a very efficient method to characterize photoresists and antireflective coatings<sup>1</sup>. Compared to more simple techniques like reflectance, ellipsometry has several advantages. First, the measurement is made on a ratio of two signals ( $R_p/R_s$  where  $R_p$  and  $R_s$  are the reflection coefficients of the two polarisations parallel and perpendicular to the incidence plane). So the measurement is independent of the source fluctuations and the accuracy of the measurement is generally better than a photometric one. There is also no need of reference sample since the measurement is self-calibrated. Finally, two independent parameters are measured simultaneously instead of one for reflectance or transmittance, which allows direct extraction of complex indices without using Kramers-Kronig methods. The measurement can be also rapid now, thanks to the development of multichannel detectors<sup>2</sup>. Photoresist behavior versus exposure dose has for example been determined by this method<sup>3</sup>. At 157nm, the layer thickness is generally smaller than for the old lithographic generations. So the correlation between thickness and indices is enhanced making more difficult the use of photometric techniques. Moreover, at shorter wavelength diffuse scattering from surfaces and contamination become more and more important so that ellipsometry becomes probably the best alternatives. On the other hand, primary lens material for projection systems will be metal fluorides such as  $\text{CaF}_2$ ,  $\text{MgF}_2$  or  $\text{LiF}$  which will require intensive characterization especially for their optical properties at 157nm. A metrologic tool capable to make photometric measurements is also more interesting.

Ellipsometers in the VUV (vacuum UV) have been demonstrated as early as 1970<sup>4</sup>. These early VUV ellipsometers utilized a vacuum chamber and synchrotron radiation for the light source. Of course, it was not a practical setup for widespread use and thus precise optical constants of many materials are not known in this range. To fill this technological gap SOPRA has decided recently to develop a new spectroscopic ellipsometer capable to work down to 145nm. The commercially available instrument has been tested recently<sup>5</sup>. Additional possibilities such as variable incidence angle and photometric measurement have also been included to fulfill the characterization requirements of this new generation of photolithography. We describe here after the instrument with numerous results related to the field of microlithography.

\* Correspondence: Email: [analyse@sopra-sa.com](mailto:analyse@sopra-sa.com); Telephone: 33 1 47 81 09 49; Fax: 33 1 42 42 29 34

## 2. EXPERIMENTAL DETAILS

### 2.1. Description of the PUV system

Two main differences appear when we want to work at 157nm. First, because of the strong molecular absorption bands in  $O_2$  and  $H_2O$  at 157nm, the entire beam path must be free of this kind of contamination. Secondly, the standard optical path used at SOPRA with a monochromator just before the detector and connected to the analyser arm of the ellipsometer by an optical fiber cannot be used. These two problems have been solved using the following solutions:

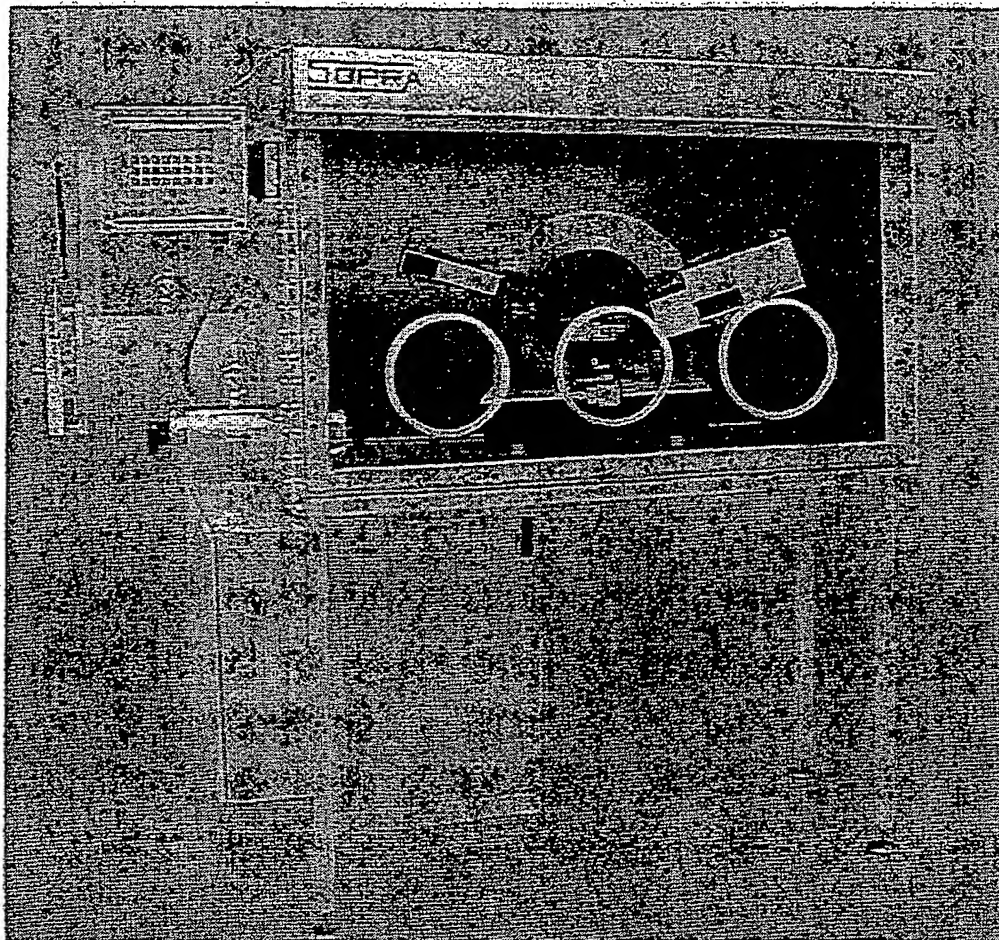


Figure 1: General view of the SOPRA Purged UV Spectroscopic Ellipsometer.

#### 2.1.1. Spectroscopic ellipsometer setup

The double monochromator is included in the polariser arm just after the deuterium lamp. This mounting ensures an optimized straight light rejection with a minimized beam path. The light beam goes through a  $MgF_2$  Rochon polarizer mounted on a stepper motor. The reflected beam passes through another Rochon analyser and is detected by a photomultiplier in photon counting mode. The two arms are mounted on a high precision goniometer. The angle of incidence can be changed automatically in the range  $7-90^\circ$ . The system works in rotating analyser mode to avoid parasitic polarisation due to the monochromator. Polarisation sensitivity of the detector is calibrated in straight line. The spectral range is 145-300nm but it can be extended in the visible range. In addition to ellipsometry, the system can make photometric measurements (reflectance and transmittance) at fixed polarisation state. Scatterometric measurements are also possible.

### 2.1.2. Purged glove box

The entire system is installed inside a glove box with continuous  $H_2O$  and  $O_2$  purification. Dry nitrogen is injected continuously in the box with automatic adjustment of the surpressure. The filters can be regenerated automatically every six months. One working face with three gloves allows adjustment of the different parts of the system, to mount the sample on the sample holder and to replace the deuterium lamp when needed. Samples up to 200mm diameter are introduced using a load lock. Residual  $H_2O$  and  $O_2$  are measured continuously. They are in the part per million ranges during normal working conditions.

## 2.2. Standard GESP system with GXR option

### 2.2.1. Spectroscopic Ellipsometry

Additional spectroscopic ellipsometry measurements are made with a commercially available SOPRA GESP (Gonio-Ellipso-Spectro-Photometer) in the visible range and around to compare with the PUV results. It is a rotating polarizer instrument with a high-resolution double monochromator and photon counting detector. The angle of incidence can be changed automatically in the range  $7-90^\circ$ . A 3mm-diameter beam is collimated from a 75W Xe lamp with a system of mirrors and passes through an  $MgF_2$  Rochon polarizer. The reflected beam passes through another Rochon analyser and is focused onto the entrance of an optical fiber connected to a prism-grating monochromator. In addition to SE measurements, reflectance, transmittance and scattering measurements can also be made with the same instrument. The wavelength range used in this study is 190-850nm but it can be extended to the near infrared region (up to 2050nm).

### 2.2.2. Grazing x-ray reflection

On the GESP instrument, a GXR option can be mounted. In this case, in addition to the ellipsometer arms, a x-ray setup is mounted on the same high precision  $\theta, 2\theta$  variable angle goniometer. It includes a ceramic fine focus x-ray tube (Copper K- $\alpha$  line at 1.54Å) cooled with water. A computer controlled stabilized high voltage supply is used at 40KV, 30mA. All safety relative to x-rays has been included. The beam is defined perpendicular to sample surface using Soller slits located just after the x-ray tube. The beam divergence is limited by interchangeable slits (or a parabolic multilayer mirror as option). A curved graphite crystal is used to monochromatize the x-ray beam after reflection on the sample surface. Standard sample holder is manually adjustable on three axes. Sample dimension can be up to 200mm diameter and 25mm thickness. The detection is made using a NaI scintillator with beryllium window and a photomultiplier tube in photon counting mode as for the standard GESP5 instrument. The dynamic range of the instrument can be extended to more than  $10^6$  using automatic Ni attenuators and optimized integration time. The system is computer controlled with a user-friendly software under Microsoft windows NT environment. Standard x-ray diffraction measurements can also be made with the same optical setup. This system is described in details with some examples of application in reference<sup>6</sup>.

## 3. EXPERIMENTAL RESULTS

We present results in three different fields. The materials for the optics of the next generation stepper are very important especially in terms of transmittance, sensitivity to contamination and deposition of antireflective coatings<sup>7-8</sup>. This subject is initiated with some ellipsometric and photometric measurements on  $CaF_2$  substrate and the results are compared to the literature. Thin oxynitride gate dielectrics have already been widely used<sup>9</sup>. In this structure the reliability at high electric field depends not only on the layer thickness but also on the nitridation level of the  $SiO_xN_y$  layer<sup>10-12</sup>. Grazing incidence x-ray reflectance and spectroscopic ellipsometry measurements are presented to deduce a very precise picture of this kind of sample. Finally different kinds of photoresist layers and antireflective coatings have been characterize and the results compared to those obtained using more standard ellipsometers.

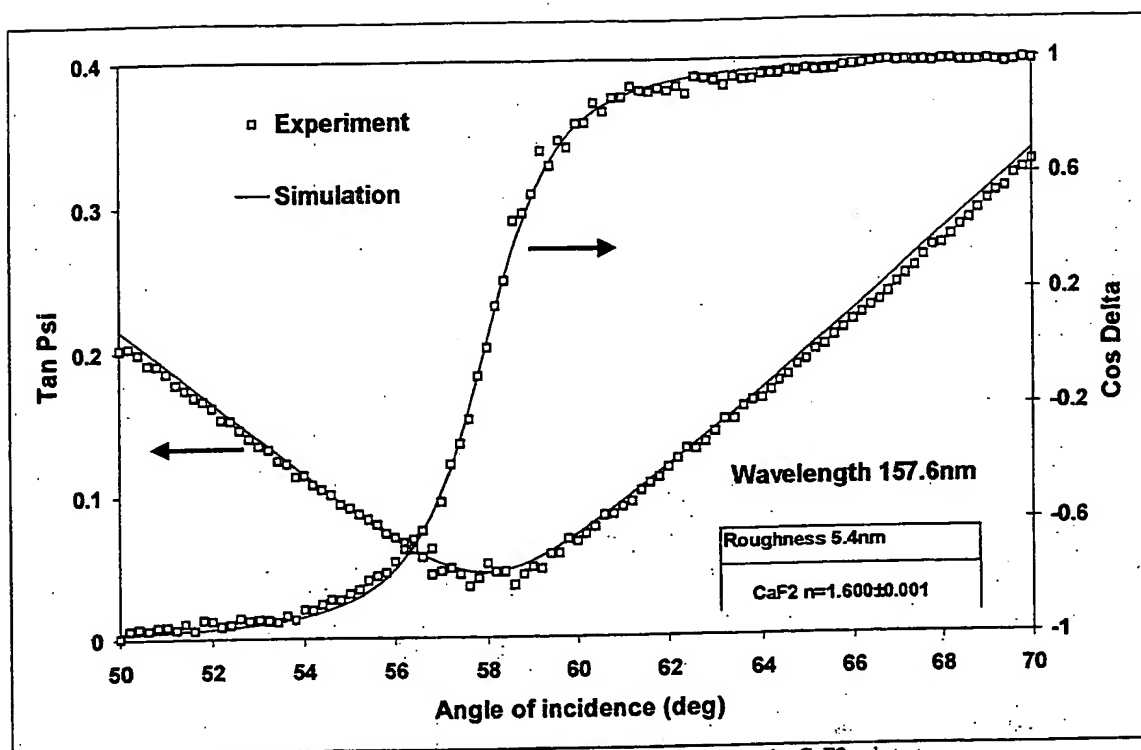


Figure 2: Analysis of the SE measurement at 157.6nm on the CaF<sub>2</sub> substrate.

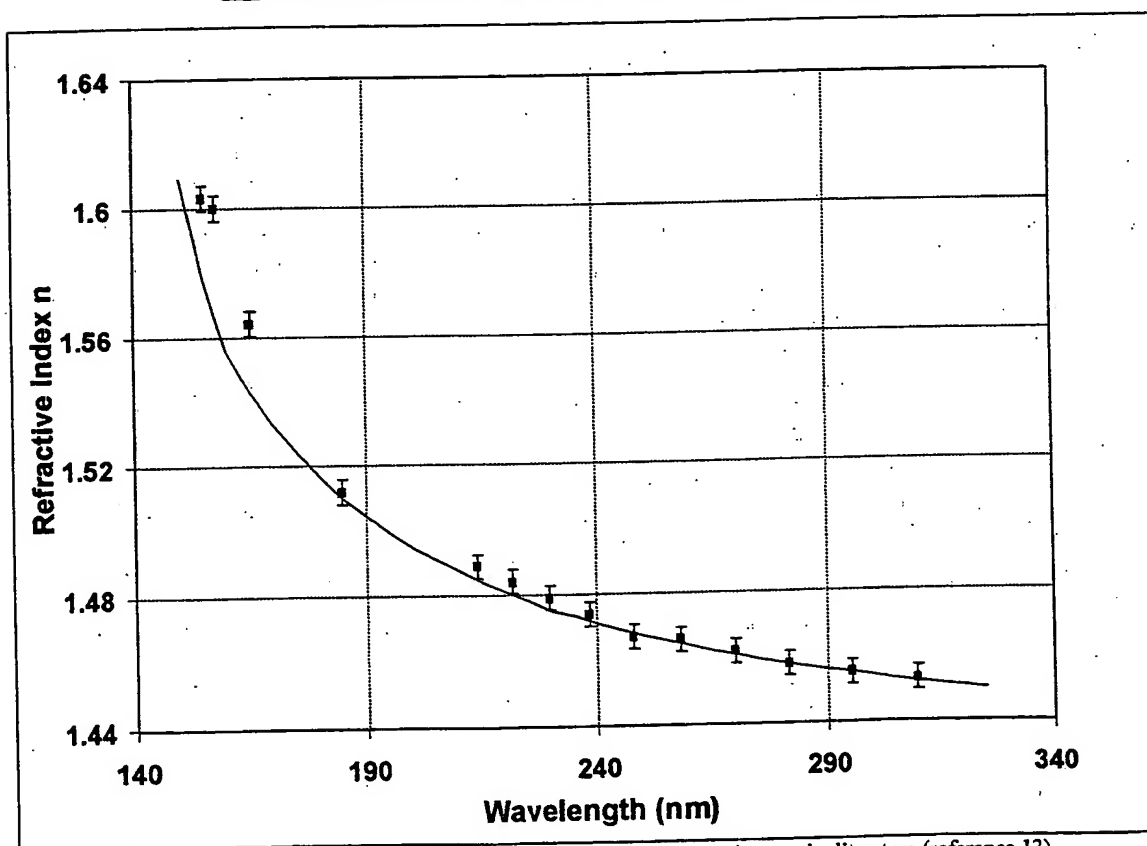


Figure 3: Measured refractive index of CaF<sub>2</sub> substrate and comparison to the literature (reference 13).

### 3.1. $\text{CaF}_2$ substrate

Variable angle SE measurements have been made at 14 different wavelengths in the range 150-300nm. The measurements are made from 50 to 70° of incidence at each wavelength. One example of experimental spectrum measured at 157.6nm is reported in Figure 2 with the simulation. A well-defined Brewster angle is detected at 58° on the two ellipsometric parameters (minimum of  $\tan\Psi$  and zero crossing value for  $\cos\Delta$ ). The shape of the  $\cos\Delta$  curve around the Brewster angle is due to the angular aperture of the measurement beam which is not negligible and must be taken into account during the analysis. Each single wavelength measurement is fitted independently using a very simple model where the refractive index of the substrate is adjusted. A top surface roughness layer is also included in the model. As can be seen on figure 2, the adjustment is very good for all the angular range. The refractive index is precisely determined at each wavelength ( $n = 1.600 \pm 0.001$  at 157.6nm from Figure 2) and also the thickness of the top surface roughness (5.3nm). The different refractive index obtained by this method at the different wavelengths are reported in Figure 3. Also shown in the figure is the optical indices from the literature<sup>13</sup>. We see that the agreement of the results is very good above 190nm. Below this value a slight discrepancy is observed. As already observed by others, in this wavelength range the contamination of the sample surface becomes critical. We think that the discrepancy of our results and the literature are mainly due to a thin contaminant layer on top of the  $\text{CaF}_2$  substrate. To check this point a transmittance measurement has been made in the same wavelength range with the new instrument. Result is reported in Figure 4 with what can be expected from a perfectly clean substrate. The discrepancy between the two transmittances is also an indication of the occurrence of a contaminant layer.

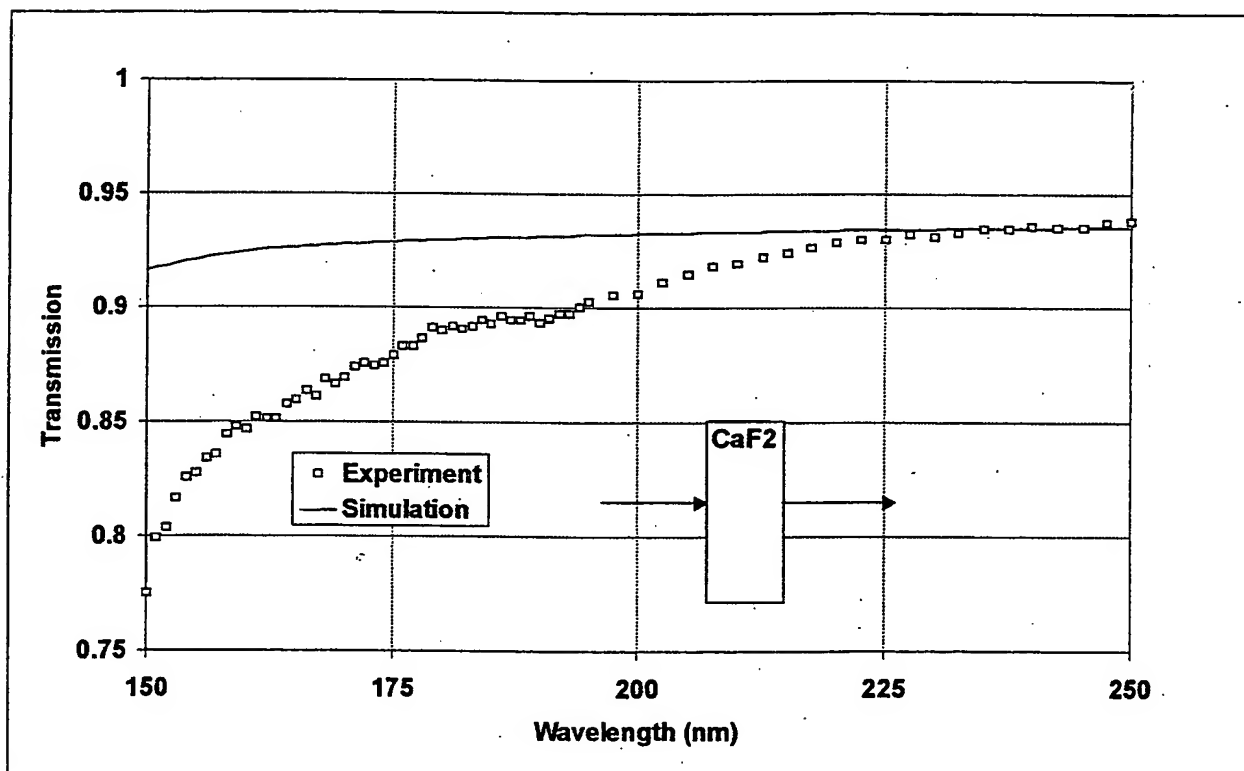


Figure 4: Transmittance of a  $\text{CaF}_2$  substrate. Simulation with perfectly transparent substrate is also included.

### 3.2. Thin oxynitride gate dielectrics

One serie of nitride/oxide gate dielectrics has been analyzed in this study. Each sample has been measured by grazing x-ray reflectance prior to the spectroscopic ellipsometry analysis. One examples of such a measurement is reported in Figure 5. In all the cases, after total reflection at very grazing angle, the x-ray beam goes through the sample and the reflectance decreases rapidly when the grazing angle is increasing. The angular position of the total reflection threshold is related to the

mean density value of the sample. With these very thin layers it cannot be used to deduce valuable informations. The optical contrast between  $\text{SiO}_2$  and crystalline silicon is very small even if it can be used to measure accurately  $\text{SiO}_2$  gate transistors [10]. The contrast between nitride and oxide is more important. It produces interference fringes which becomes detectable at  $1.5\text{-}2^\circ$ . The angular position of these fringes is characteristic of the thickness of the layers and the amplitude of the fringes is related to the index contrast between the layers (and then their composition). For each measurement we have applied a two layers model adjusting at the same time the different layer thicknesses, the x-ray indices and the mean roughness of the stack. We neglect the thin bottom  $\text{SiO}_2$  layer since its optical index contrast is very small compare to the  $\text{Si}_3\text{N}_4$  layer and very close to the silicon substrate. The simulation is also reported in Figure 5. We can notice that the adjustment is very good along all the angular range. The incertitude associated to the different thicknesses is quite small (less than  $0.1\text{nm}$ , see results summarized in Table I). The two interference fringes detectable on this sample are in particular very well fitted. In table I, the GXR results for all the samples are summarized. We can see that incertitude associated to the GXR thicknesses is good except in the case of samples 5 and 7 where the contrast between oxide and nitride layers is too small due to low relative concentration of N versus O, to give well defined interference fringes. The mean roughness is small for all samples.

The same samples have been measured by SE in the  $1.5\text{-}8.2\text{eV}$  ( $150\text{-}850\text{nm}$ ) at  $75^\circ$  of incidence angle. The PUV range is covered by the new instrument ( $150\text{-}300\text{nm}$ ) and the standard range by a conventional GESP instrument ( $190\text{-}850\text{nm}$ ). The agreement between the two measurements is very good as shown in figure 6 where the phase shift ( $\cos\Delta$  parameter) of the three nitride/oxide gate dielectrics is reported. This parameter is the most sensitive to any change of layer thickness and composition of the nitride/oxide gate dielectrics. Large differences can be detected between the three samples as expected from GXR measurements (see Figure 5). Analysis of the SE results has been made using the following procedure. The thicknesses of the top  $\text{SiO}_2$  and  $\text{SiO}_x\text{N}_y$  layers are fixed to the GXR values. A bottom  $\text{SiO}_2$  layer is added and its thickness is adjusted. The composition of the  $\text{SiO}_x\text{N}_y$  layer is also adjusted (assuming a Bruggmann mixture of the optical indices of  $\text{SiO}_2$  and  $\text{Si}_3\text{N}_4$  from the database). Results are summarized in Table I. We can notice that the incertitude associated to the  $\text{Si}_3\text{N}_4$  content is small (less than 5% except for the two samples with small optical contrast).

On Table I, x-ray photoemission spectroscopy (XPS) measurements of the N/O ratio of the same samples are also reported. We can notice the very good agreement between these chemical results and the combined GXR/SE measurement of the  $\text{SiO}_x\text{N}_y$  composition. In fact the coherency of the results is very good even for the two samples with less optical contrast (sample 5 and 7) for which XPS confirms the low nitrogen content. Our combined analysis is then validated a posteriori. We must point out that a standard analysis on the SE measurements alone is not so coherent. The reason is the high degree of correlation between thickness and composition for these very thin layers and the occurrence of more than one layer on the silicon substrate. The situation is different for example for  $\text{SiO}_2$  gate oxide layer where the optical index is known. Otherwise, for more complex nitride/oxide structures the GXR informations are extremely important for the SE analysis<sup>14</sup>.

	Grazing x-ray reflectance			Spectroscopic ellipsometry		XPS
	Top $\text{SiO}_2$ (nm)	$\text{Si}_x\text{N}_y\text{O}_z$ (nm)	Roughness (nm)	Bottom $\text{SiO}_2$ (nm)	$\text{Si}_3\text{N}_4$ content (%)	N/O (%)
Sample 1	$0.57\pm0.04$	$1.97\pm0.02$	$0.15\pm0.02$	$0.80\pm0.04$	$30\pm4$	38
Sample 2	$0.99\pm0.05$	$2.12\pm0.03$	$0.17\pm0.02$	$1.27\pm0.05$	$42\pm5$	70
Sample 3	$0.91\pm0.09$	$2.23\pm0.08$	$0.21\pm0.01$	$0.71\pm0.03$	$54\pm3$	79
Sample 4	$0.82\pm0.15$	$2.48\pm0.06$	$0.14\pm0.01$	$0.49\pm0.05$	$27\pm3$	32
Sample 5	$0.62\pm0.9$	$2.45\pm0.8$	$0.18\pm0.1$	$0.35\pm0.1$	$19\pm7$	16
Sample 6	$0.58\pm0.5$	$2.01\pm0.2$	$0.16\pm0.05$	$1.03\pm0.05$	$24\pm4$	24
Sample 7	$0.57\pm1.2$	$2.01\pm0.9$	$0.18\pm0.1$	$0.24\pm0.1$	$14\pm7$	15

Table I: Summarized results obtained by GXR, SE and XPS on nitride/oxide gate dielectrics



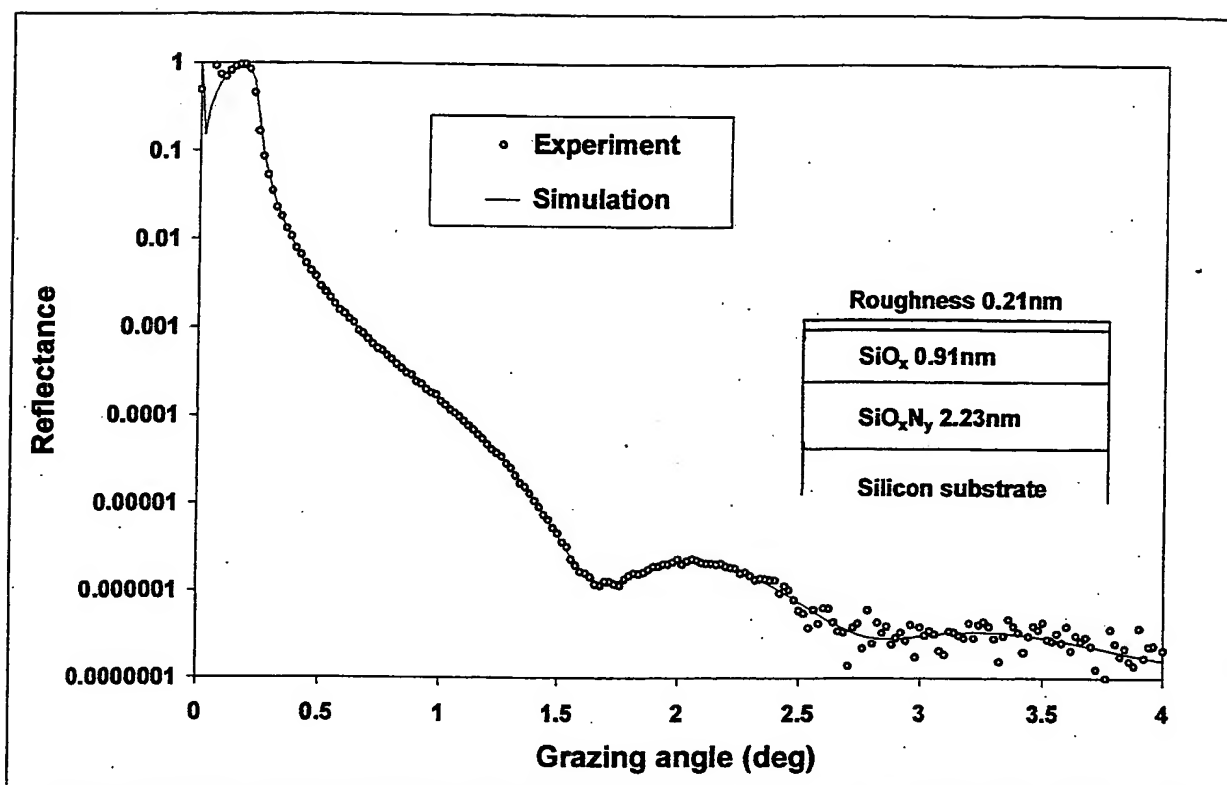


Figure 5: GXR analysis of one oxide/nitride gate dielectric (sample 3 of Table I). Model used for simulation is also reported.

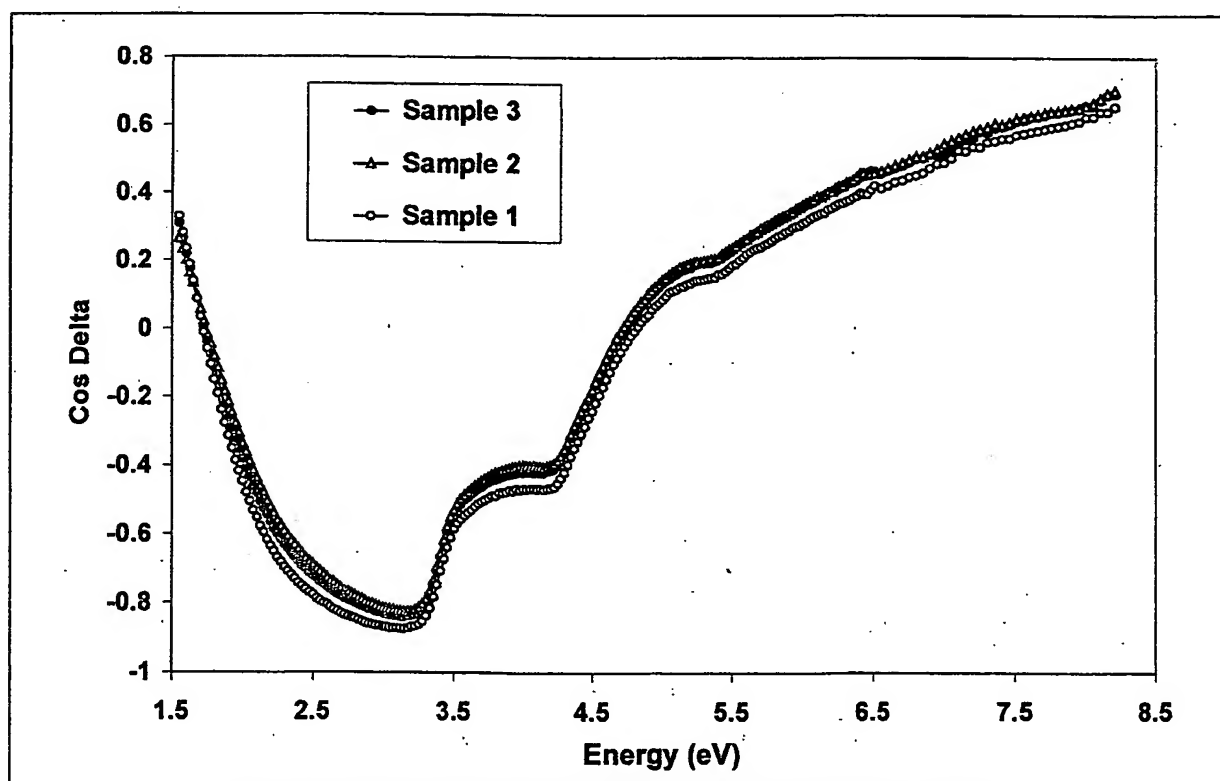


Figure 6: Experimental SE spectra of three oxide/nitride gate dielectrics up to 8.2nm.



### 3.3. Different kinds of photoresists

Photoresists have been intensively studied at 248nm and 193nm using spectroscopic ellipsometry<sup>15</sup>. It is now possible to make the same work at 157nm. Here after we present different kinds of results in the field.

#### 3.3.1. Precise analysis of two photoresist films

Two kinds of photoresist for F2 line (157nm) have been analyzed using the PUV system and also a standard GESPE instrument. In both cases, spectroscopic ellipsometry measurements have been made at different angles of incidence (65, 70 and 75°) in the wavelength range 150-330nm for the PUV and 190-850nm for the GESPE system. One example of such measurement in the PUV range is reported in Figure 7. In this case a very well defined interference fringe appear around 230nm. The optical indices are extracted using a procedure described in details elsewhere. The infrared part of the GESPE measurement is fitted using a dispersion law for the optical index of the photoresist layer and assuming that the layer is completely transparent. Then using the thickness determined by this method, the optical indices are extracted point by point in the entire wavelength range. At each wavelength the optical indices are adjusted for all the incidence angles. Results obtained independently on the two instruments are summarized in Figure 8. One can see that, first the layer is really transparent in the infrared range (below 3eV), and secondly that the coherence between the two instruments is very good in the common wavelength range.

The same kind of analysis has been made on another kind of photoresist. The optical indices obtained with the two instruments are also reported in Figure 9. Here also the coherency between the two instruments is very good particularly in the shape of the absorption peaks at 4.5eV and 6.5eV. In both cases, the optical indices obtained in the PUV range can be considered with a high degree of confidence.

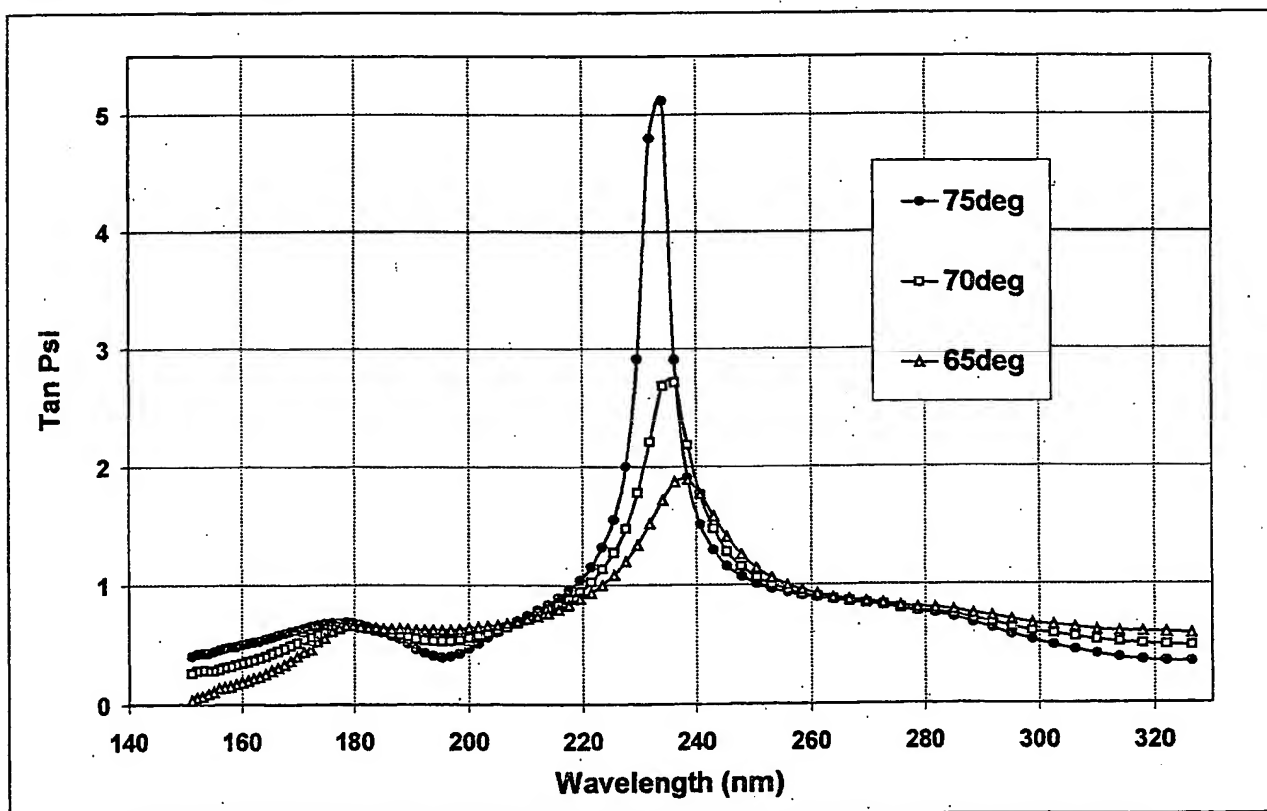


Figure 7: Experimental SE spectra of a photoresist layer on silicon substrate at three different incidence angles.

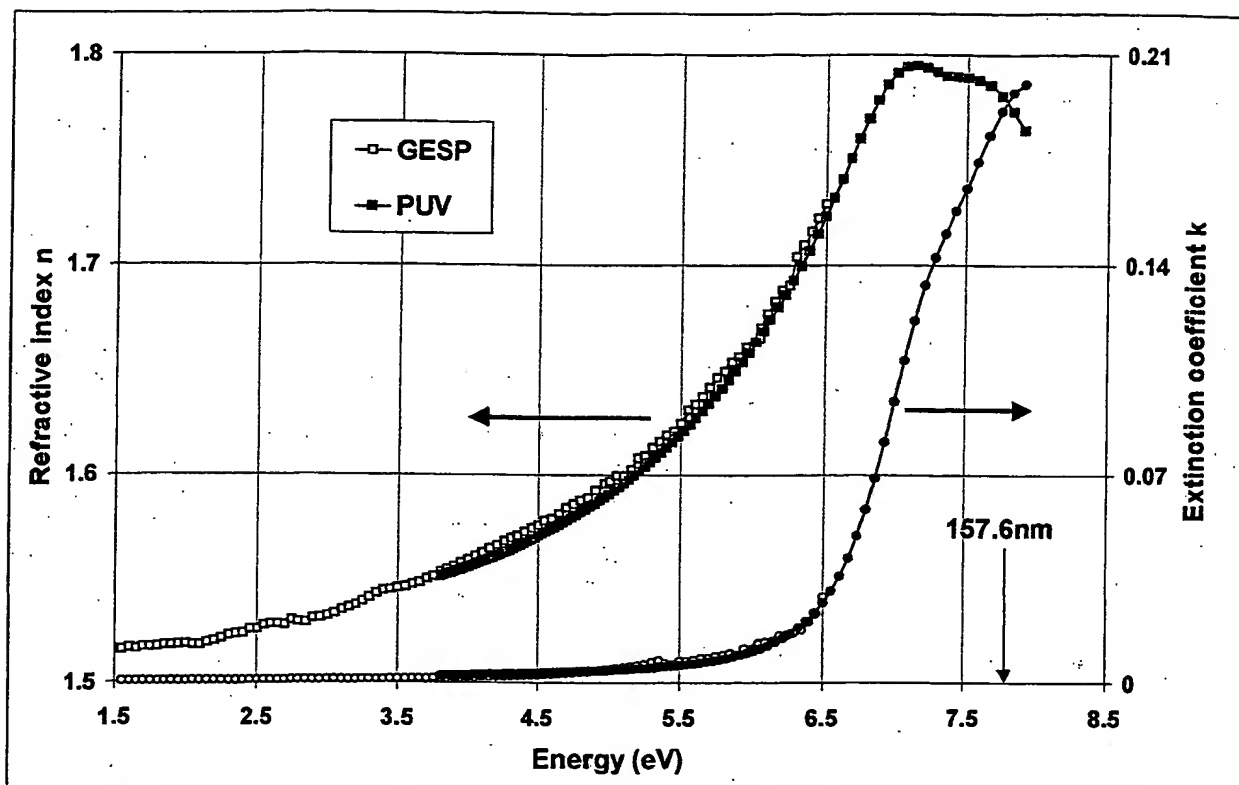


Figure 8: Optical indices of the photoresist layer of figure 7. Analysis is made using PUV and GESP instruments.

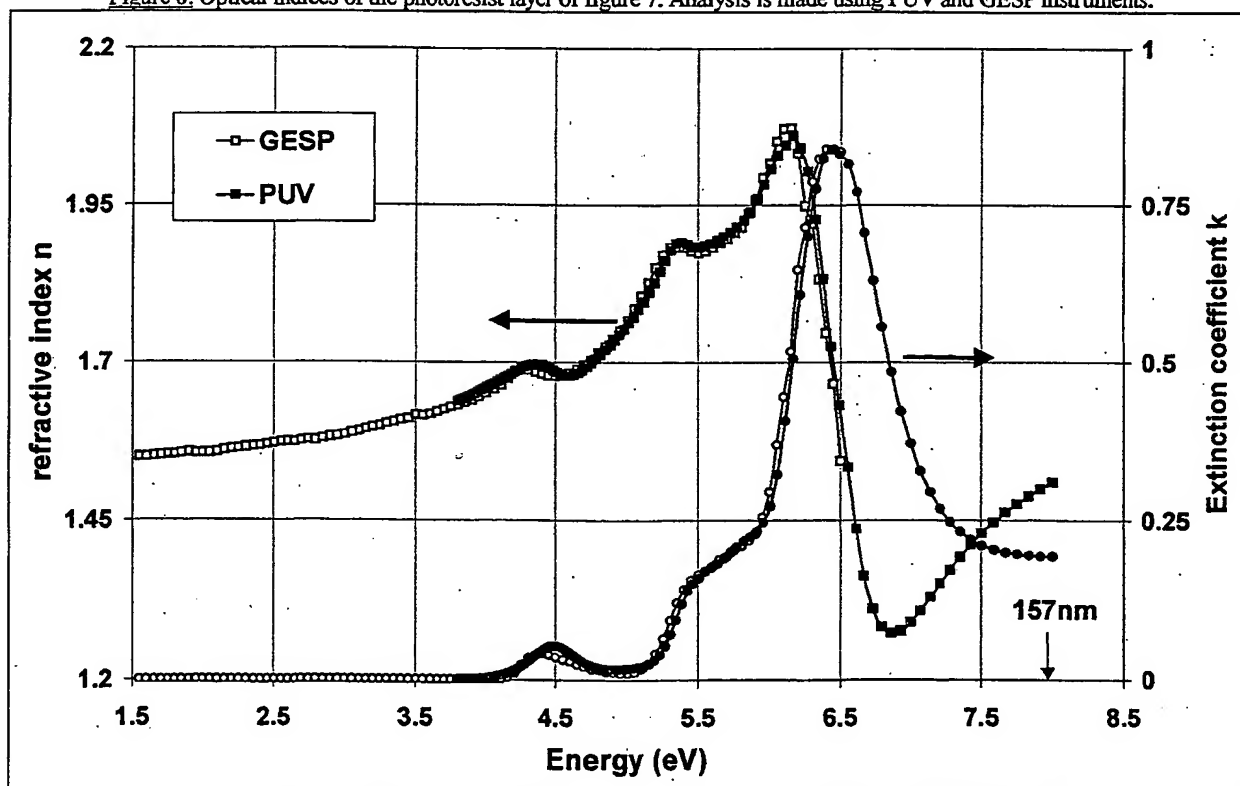


Figure 9: Optical indices of a photoresist layer. Analysis is made using PUV and GESP instruments.

### 3.3.2. PUV of different kinds of photoresist and ARC films

On figure 10, we have reported the optical indices of different photoresist layers and one ARC (Anti Reflective Coating) measured in the PUV range from 150 to 330nm. Four kinds of resist for i-line, ArF line, KrF line and F2 line are reported with one ARC for F2 line. From these high accuracy indices, optimization of the lithographic structures can be easily obtained at each wavelength.

## 4. CONCLUSION

We have presented a new metrology system capable to measure optical properties of substrates and thin films in the range 145-300nm. This new system is a spectroscopic ellipsometer mounted inside a purged glove box to suppress strong absorption by  $O_2$  and  $H_2O$  gases. In addition to spectroscopic ellipsometry, photometric (reflectance and transmittance) and scatterometric measurements are also possible. Experimental results on  $CaF_2$  substrate, thin oxynitride gate dielectrics and photoresist layers have been presented. The results obtained with the new instrument are coherent with the literature and also with independent measurements: spectroscopic ellipsometry realized with the standard SOPRA GESP instrument and grazing x-ray reflection measurements in the case of thin oxynitride gate dielectrics. The addition of a GXR option inside the PUV system is under study. We think that x-ray informations will be helpful in this wavelength range due to the limited values of the layer thickness and the great sensitivity to roughness and contaminations.

## 5. ACKNOWLEDGMENTS

SEMATECH (United States), SELETE (Japan) and TOKYO-OHKA (Japan) are kindly acknowledged for providing samples.

## 6. REFERENCES

1. P.Boher, J.P.Piel, C.Defranoux, J.L. Stehle, L.Hennet, SPIE vol. 2729 (1996)
2. P. Boher, J.L. Stehle, Materials. Science and Engineering, B37, 116 (1996)
3. P. Boher, C. Defranoux, J.P. Piel, J.L. Stehle, SPIE, vol. 3678, p. 126 (1999)
4. J. Barth, R.L. Johnson, M. Cardona, Chapter 10 in Handbook of Optical Constants of Solids II, ed. Palik, Academic Press (1991)
5. P. Boher, J.P.Piel, P. Evrard, J.L. Stehle, MRS Fall meeting, november 29 – december 3 (1999)
6. P. Boher, J.L. Stehle, Phys. Stat. Sol., 170, pp. 211-220 (1998)
7. T.M. Bloomstein, M. Rothschild, R.R. Kunz, D.E. Hardy, R.B. Goodman, S.T. Palmacci, J. Vac. Sci. Technol., B16, 3154 (1998)
8. T.M. Bloomstein, V. Liberman, M. Rothschild, SPIE vol. 3676, 342 (1999)
9. K. Kobayashi, J. Electrochem. Soc., vol. 139, N°5, p. 1693 (1992)
10. L.K. Han, IEEE Electron device letters, vol. 16, N°8, p. 348 (1995)
11. G.Q. Lo, IEEE Electron device letters, vol. 13, N°7 (1992)
12. M.K. Mazumder, J. Electrochem. Soc. Vol. 143, N°1, p. 368 (1996)
13. D.F. Bezuidenhout, Handbook of Optical Constants of Solids II, ed. Palik, Academic Press, p. 815 (1991)
14. P. Boher, J.P.Piel, J.L. Stehle, MRS Fall meeting, november 29 – december 3 (1999)
15. P. Boher, C. Defranoux, S. Bourtaut, J.L. Stehle, SPIE vol. 3677, 845 (1999)

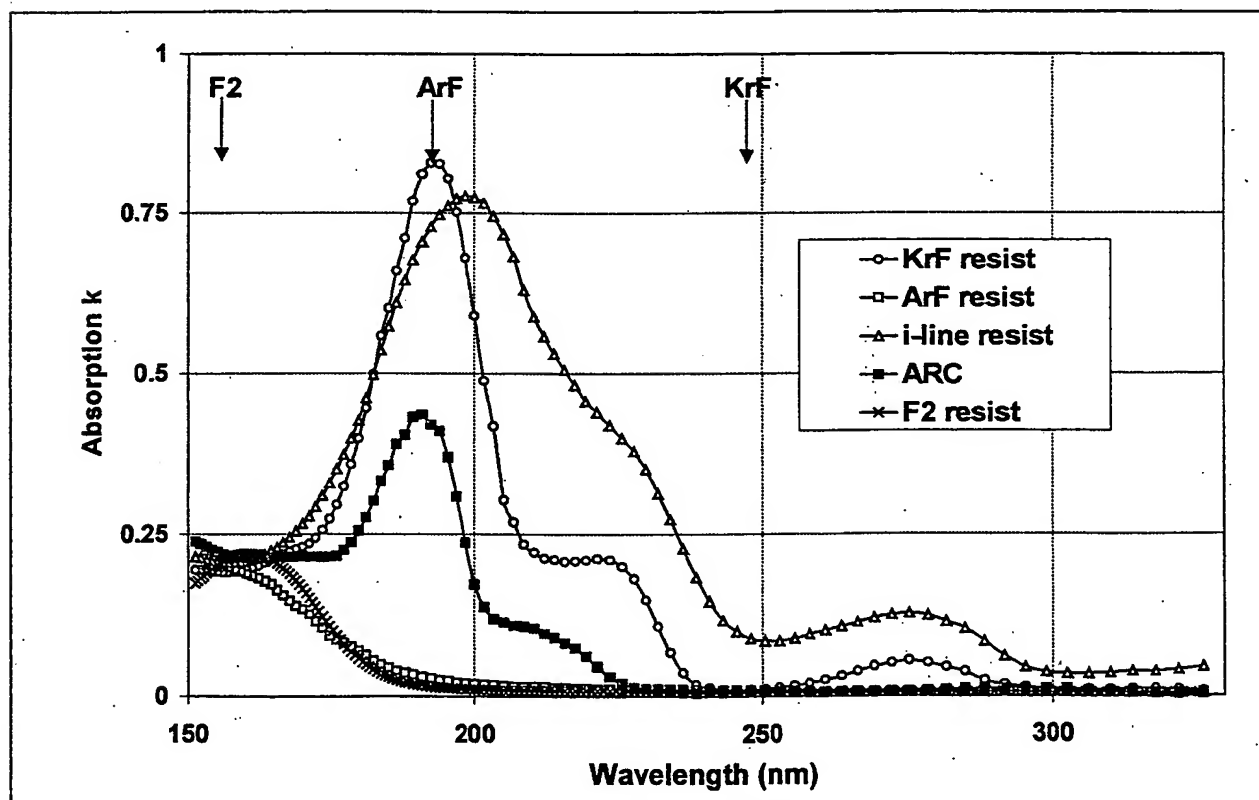
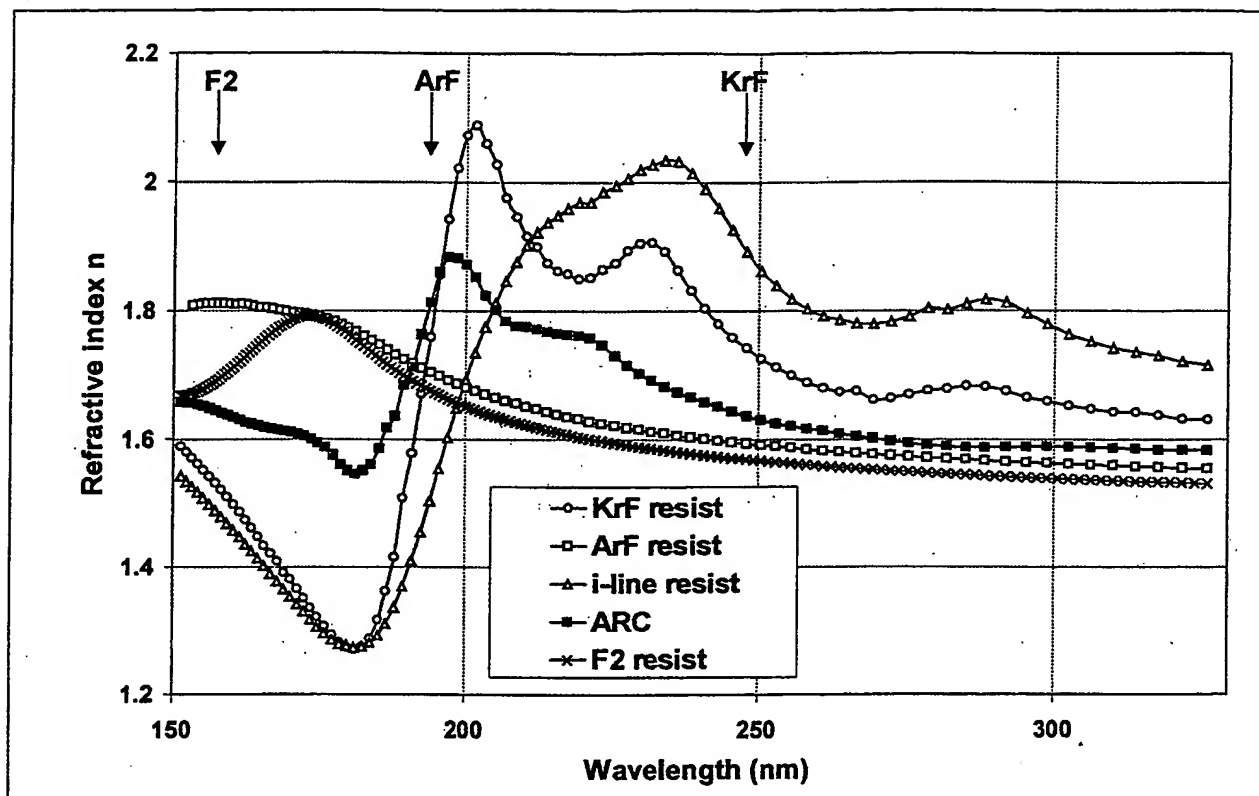


Figure 10: Optical indices of a various photoresist materials measured by the new PUV system.

**This Page is Inserted by IFW Indexing and Scanning  
Operations and is not part of the Official Record**

**BEST AVAILABLE IMAGES**

Defective images within this document are accurate representations of the original documents submitted by the applicant.

Defects in the images include but are not limited to the items checked:

- ☒ **BLACK BORDERS**
- ☐ **IMAGE CUT OFF AT TOP, BOTTOM OR SIDES**
- ☐ **FADED TEXT OR DRAWING**
- ☐ **BLURRED OR ILLEGIBLE TEXT OR DRAWING**
- ☐ **SKEWED/SLANTED IMAGES**
- ☒ **COLOR OR BLACK AND WHITE PHOTOGRAPHS**
- ☐ **GRAY SCALE DOCUMENTS**
- ☐ **LINES OR MARKS ON ORIGINAL DOCUMENT**
- ☐ **REFERENCE(S) OR EXHIBIT(S) SUBMITTED ARE POOR QUALITY**
- ☐ **OTHER:** \_\_\_\_\_

**IMAGES ARE BEST AVAILABLE COPY.**

**As rescanning these documents will not correct the image problems checked, please do not report these problems to the IFW Image Problem Mailbox.**